The FASEB Journal article fj.10-155846. Published online March 24, 2010.

Xanthohumol-induced transient superoxide anion radical formation triggers cancer cells into apoptosis *via* a mitochondria-mediated mechanism

Julia Strathmann,* Karin Klimo,* Sven W. Sauer,† Jürgen G. Okun,† Jochen H. M. Prehn,‡ and Clarissa Gerhäuser*

*German Cancer Research Center, Heidelberg, Germany; †University Children's Hospital, Heidelberg, Germany; and ‡Royal College of Surgeons in Ireland, Dublin, Ireland

ABSTRACT **Oxidative stress and increased release of reactive oxygen species (ROS) are associated with apoptosis induction. Here we report ROS-mediated induction of apoptosis by xanthohumol (XN) from hops. XN at concentrations of 1.6–25 μM induced an immediate and transient increase in superoxide anion radical ($O_2^{-\cdot}$) formation in 3 human cancer cell lines (average±SD EC_{50} of maximum $O_2^{-\cdot}$ induction=3.1±0.8 μM), murine macrophages (EC_{50}=4.0±0.3 μM), and BPH-1 benign prostate hyperplasia cells (EC_{50}=4.3±0.1 μM), as evidenced by the $O_2^{-\cdot}$-specific indicator dihydroethidium. MitoSOX Red costaining and experiments using isolated mouse liver mitochondria (EC_{50}=11.4±1.8 μM) confirmed mitochondria as the site of intracellular $O_2^{-\cdot}$ formation. Antimycin A served as positive control (EC_{50}=12.4±0.9 μM). XN-mediated $O_2^{-\cdot}$ release was significantly reduced in BPH-1 ρ^0 cells harboring nonfunctional mitochondria (EC_{50}>25 μM) and by treatment of BPH-1 cells with vitamin C, *N*-acetylcysteine (NAC), or the superoxide dismutase mimetic MnTMPyP. In addition, we demonstrated a rapid 15% increase in oxidized glutathione and a dose-dependent overall thiol depletion within 6 h (IC_{50}=24.3±11 μM). Respiratory chain complexes I–III were weakly inhibited by XN in bovine heart submitochondrial particles, but electron flux from complex I and II to complex III was significantly inhibited in BPH-1 cells, with IC_{50} values of 28.1 ± 2.4 and 24.4 ± 5.2 μM, respectively. Within 15 min, intracellular ATP levels were significantly reduced by XN at 12.5 to 50 μM concentrations (IC_{50}=26.7±3.7 μM). Concomitantly, XN treatment caused a rapid breakdown of the mitochondrial membrane potential and the release of cytochrome *c*, leading to apoptosis induction. Pre- or coincubation with 2 mM NAC and 50 μM MnTMPyP at various steps increased XN-mediated IC_{50} values for cytotoxicity in BPH-1 cells from 6.7 ± 0.2 to 12.2 ± 0.1 and 41.4 ± 7.6 μM, and it confirmed XN-induced $O_2^{-\cdot}$ as an essential trigger for apoptosis induction. In summary, we have identified mitochondria as a novel cellular target of XN action, resulting in increased $O_2^{-\cdot}$ production, disruption of cellular redox balance and mitochondrial integrity, and subsequent apoptosis.—Strathmann, J., Klimo, K., Sauer, S. W., Okun, J. G., Prehn, J. H. M., Gerhäuser, C. Xanthohumol-induced transient superoxide anion radical formation triggers cancer cells into apoptosis *via* a mitochondria-mediated mechanism. *FASEB J.* 24, 000–000 (2010). www.fasebj.org**

Key Words: polyphenols · oxidative stress · chemoprevention

Reactive oxygen species (ROS), such as hydrogen peroxide (H_2O_2), superoxide anion radicals ($O_2^{-\cdot}$), and hydroxyl radicals (OH·), are generated in cells by various pathways. Several cellular enzymatic complexes have been identified as sites of ROS production, such as NADPH cytochrome P450 reductases, hypoxanthine/xanthine oxidase, NADPH oxidase, lipoxygenase, peroxidases, and cyclooxygenases (1). However, mitochondria are believed to be the major source of ROS in aerobic cells (2, 3), as during oxidative phosphorylation ~1–2% of all transported electrons escape and reduce O_2 to $O_2^{-\cdot}$ (4, 5). Recently, ROS have been identified as key redox regulators of cellular signaling cascades, metabolic processes, and transcription factors.

Redox regulation has been shown to play a crucial role in cell survival by the activation of kinases, oncogenic Ras signaling, lipid metabolism, calcium signaling, and activation of transcription factors, such as AP-1, NFκB, and p53, which are tightly regulated and balanced by the cellular antioxidant system (5–7). Macrophages, neutrophils, and eosinophils are an additional source of endogenous ROS production and fight pathogens by a transient respiratory burst of oxidative stress, indicating another crucial involvement of ROS in cellular maintenance (8). Nevertheless, chronic oxidative stress frequently occurs as a consequence of an imbalanced intracellular redox status, promoting a variety of pathologies, such as malignant diseases, type II diabetes, atherosclerosis, chronic inflammation, ischemia/reperfusion injury, and many neurodegenerative diseases (9). Acute high ROS levels

[1] Correspondence: German Cancer Research Center, Im Neuenheimer Feld 280, 69120 Heidelberg, Germany. E-mail: c.gerhauser@dkfz.de

doi: 10.1096/fj.10-155846

damage cellular compartments, leading to inactivation and malfunction of various enzymes, as excess amounts of $O_2^{-\cdot}$ directly oxidize and inactivate iron-sulfur complex-containing proteins. Mitochondrial dysfunction has been shown to play a key role in the induction of apoptosis (10, 11). Impaired mitochondrial functions lead to the suppression of mitochondrial metabolism, imbalanced mitochondrial membrane potential, reduced respiration, and oxidative phosphorylation (6), and finally trigger cells into apoptosis (12).

This basic knowledge on ROS signaling has been utilized for the development of novel therapeutic applications in human diseases. Besides treatment of patients with antioxidants to prevent cardiovascular and neurodegenerative diseases and cancer (13, 14), recent research revealed that cells with an imbalanced redox homeostasis are more susceptible to oxidative stress-induced apoptosis than normal cells. Therefore, ROS-generating drugs might be very effective in treating malignant diseases by disrupting mitochondrial functions and inducing apoptosis (15). Several dietary polyphenols have been well investigated with respect to antioxidant action, and mechanistic modes of activity have been described previously (16). However, more recent publications state that in addition to antioxidant potential, many polyphenols exert prooxidant properties at low concentrations (17) and therefore might selectively trigger cells with an imbalanced redox homeostasis into apoptosis by the induction of excessive ROS formation (18).

One natural antioxidative polyphenol is xanthohumol (XN), a prenlyated chalcone derived from hops (*Humulus lupulus* L.). XN exerts a broad spectrum of chemopreventive actions, such as inhibiting the initiation, promotion, and progression of malignant tumors *in vitro* and *in vivo* (19, 20). XN has antiproliferative properties and induces apoptosis in several cancer cell lines, including leukemia cell lines, prostate cancer, and hepatoma cell lines (summarized in ref. 21). Down-regulation of Bcl-2 protein expression; activation of caspases-3, -7, -8, and -9; and poly(ADP-ribose)polymerase (PARP) cleavage were found to contribute to apoptosis induction *via* both the extrinsic as well as the intrinsic apoptotic pathway in cultured human colon cancer cells (22). Induction of apoptosis and differentiation by XN in preadipocytes were linked to the induction of ROS (23, 24). Recently, XN has been reported to activate the proapoptotic arm of the unfolded protein response in chronic lymphocytic leukemia (25).

The aim of the present study was to elucidate mechanisms involved in putative prooxidant activities of XN as a trigger of antiproliferative activity. We have monitored the formation of superoxide anion radicals ($O_2^{-\cdot}$) by XN and measured disruption of the intracellular redox balance and inhibition of the complexes of the mitochondrial respiratory chain. Further, we investigated mitochondrial integrity *via* the loss of mitochondrial membrane potential, release of cytochrome *c* (cyt *c*), and induction of apoptosis. Our results suggest that XN shares functional similarities with "mitocans," a newly defined class of therapeutic and preventive drugs that selectively target mitochondria, destabilize them, and therefore efficiently kill cells with an imbalanced redox homeostasis (26).

MATERIALS AND METHODS

Chemicals

XN (CAS 6754-58-1) was obtained as hop-derived ethanolic extract with 80% purity (Hallertauer Hopfenverwertungsgesellschaft, Mainburg, Germany) and purified by silica gel column chromatography with *n*-hexane/ethyl acetate solvent essentially as described previously (19). Purity measured by HPLC was >99%. RPMI 1640 and DMEM, FBS, and trypsin/EDTA were purchased from Invitrogen (Karlsruhe, Germany). Manganese (III) tetrakis(1-methyl-4-pyridyl)porphyrin (MnTMPyP) was from A.G. Scientific, Inc. (San Diego, CA, USA). All materials required for flow cytometry were purchased from Becton Dickinson (Franklin Lakes, NJ, USA). Anti-cyt *c* antibody was from Clontech (San Diego, CA, USA), and anti-PARP (556362) antibody was from BD Pharmingen (Heidelberg, Germany). PCR Immolase *Taq* polymerase was obtained from Bioline (Taunton, MA, USA), deoxynucleotide triphosphates were from Eppendorf (Hamburg, Germany), and primers were synthesized by Sigma-Aldrich (Taufkirchen, Germany). Materials and equipment for gel electrophoresis were from Bio-Rad (Munich, Germany). All other chemicals were purchased from Sigma-Aldrich or as stated otherwise. FVB/N mice were purchased from Charles River Wiga (Sulzfeld, Germany) and housed in a controlled environment at 20°C on an illumination schedule of 12 h light and darkness each day.

Cell culture

BPH-1 cells, derived from human benign hyperplasia, were cultured in RPMI 1640 medium supplemented with 10% charcoal-stripped fetal bovine serum (FBS) and 10 μg/ml hydrocortisone, 1 μg/ml insulin, 50 ng/ml testosterone, and 5 μg/ml transferin, as described previously (27). Cyt *c* GFP-labeled MCF-7 cells were established by Dussmann *et al.* (28) and grown in DMEM, supplemented with 10% FBS at 37°C and 5% CO_2 in a humidified atmosphere. Both cell lines were seeded at a density of 5×10^4 cells/ml.

Determination of $O_2^{-\cdot}$ in cell culture and isolated mouse liver mitochondria

Cells were seeded in 96-well plates and grown overnight. After removal of cell culture medium, cells were washed with PBS, and 190 μl of 25 μM dihydroethidium (DHE) dissolved in PBS was added to each well. Immediately before the measurement was started, 10 μl of XN, other compounds as indicated, or solvent control (10% DMSO, 0.5% final concentration) was added, and the time-dependent increase in fluorescence (DHE ex/em: 530/620 nm) was measured using a CytoFluor series 4000 multiwell plate reader (PerSeptive Biosystems, Freiburg, Germany) for 20 min at 37°C.

To measure transient $O_2^{-\cdot}$ formation by XN, cells were seeded in 96-well plates, grown overnight, and treated with 12.5 μM XN for increasing time points as indicated. Then, cells were washed with PBS once, and 200 μl of 25 μM DHE dissolved in PBS was added to each well. Increase in fluorescence (DHE ex/em: 530/620 nm) was measured using a

CytoFluor series 4000 multiwell plate reader (PerSeptive Biosystems) for 20 min at 37°C.

Mitochondria were isolated from livers of male FVB/N mice, 4–6 mo of age, that were starved overnight, essentially as described earlier (29). To determine $O_2^{-\cdot}$ formation in isolated mitochondria, mitochondria were suspended in 190 μl warm PBS containing 25 μM DHE to a final protein concentration of 0.3 mg/ml. Immediately before the measurement was started, 10 μl of XN, other compounds as indicated, or solvent control (10% DMSO and 0.5% final concentration) was added, and the time-dependent increase in fluorescence (DHE ex/em: 530/620 nm) was measured using a CytoFluor series 4000 multiwell plate reader for 20 min at 37°C.

Determination of H_2O_2

For the determination of H_2O_2, an Amplex Red hydrogen peroxide/peroxidase assay kit (Invitrogen) was utilized according to the manufacturer's instructions. In cell-free incubations, cell culture medium was mixed with Amplex red dye, horseradish peroxidase (HPR), and XN or (−)-epigallocatechin-3-gallate as positive control, respectively. Alternatively, Amplex Red dye and HPR were added to cultured BPH-1 cells, and the release of H_2O_2 was measured accordingly. H_2O_2 levels were quantified in comparison with a H_2O_2 standard curve.

Inhibition of XN induced $O_2^{-\cdot}$ formation

Cells were seeded in 96-well plates, grown overnight, and washed with PBS once. Then, 190 μl of warm PBS, containing ascorbic acid or *N*-acetylcysteine (NAC) as indicated, and 25 μM DHE was added to each well. Immediately before fluorescent measurements were started, XN (10 μl, freshly dissolved in 10% DMSO/RPMI cell culture medium, supplemented with 10% FBS, 10 μM final concentration) or solvent control (10% DMSO, 0.5% final concentration) was added. Time-dependent increase in fluorescence was monitored >20 min. To measure inhibition of $O_2^{-\cdot}$ formation by the SOD mimetic MnTMPyP, BPH-1 cells were preincubated with MnTMPyP dissolved in cell culture medium for 1 h. Then, plates were washed once with PBS and treated as described above. The rate of increase in fluorescence of cells treated with 10 μM XN alone was set as 100% and inhibition by antioxidants and MnTMPyP was calculated accordingly.

Determination of total, oxidized, and reduced thiols

To determine total thiol levels, BPH-1 cells were seeded in 96-well plates, grown overnight, and treated with increasing XN concentrations (dissolved in DMSO, final solvent concentration 0.5%) for 6 h. Then, cells were once washed with PBS and total sulfhydryl (SH) content per well was determined using 5,5′-dithiobis(nitrobenzoic acid) (Ellman's reagent) as described previously (30). To measure oxidized and reduced thiols, BPH-1 cells were seeded in 10-cm cell culture dishes (5×10^4 cells/ml, 10 ml/dish) and grown overnight as described above. Then, medium was changed, and XN was added at increasing concentrations, as indicated. DMSO was used as a solvent control (0.1% final concentration). After incubation for various time intervals as described, cells were washed with PBS, collected in 250 μl PBS, and snap-frozen in liquid nitrogen. After thawing and removal of cellular fragments by centrifugation (14,000 *g* max, 10 min, 4°C), the total SH content of cell lysates was determined (30). To measure total oxidized thiol levels using GSSG as a standard, free SH groups were masked with 1.25% 2-vinylpyridine, dissolved in 125 mM Na_2HPO_4 supplemented with EDTA 6.3 mM (pH 7.5,) for 1 h, and then processed as described previously (30). Reduced thiol levels were calculated by the difference of total SH and GSSG levels. All oxidized and reduced thiol concentrations were normalized to the total protein content.

Fluorescence microscopy images of cyt *c* GFP-MCF-7

Cyt *c* GFP-MCF-7 cells were seeded in chamber slides (Nunc, Rochester, NY, USA) at 5×10^4 cells/ml in DMEM, supplemented with 10% FBS, and grown overnight. Cell culture medium was changed to phenol red-free DMEM plus 10% FBS. To measure mitochondrial $O_2^{-\cdot}$ formation, cyt *c* GFP-MCF-7 cells were first stained with Hoechst 33342 (1 μg/ml) for 10 min, and then 25 μM XN was added and incubated for 10 min. Medium was disposed, cells were washed once with PBS, and cell culture medium containing 5 μM MitoSOX Red was added. After 5 min incubation, confocal images were taken (MitoSOX Red ex/em: Ar 514/580 nm). For time-lapse imaging, cyt *c* GFP-MCF-7 cells were first stained with Hoechst 33342 (1 μg/ml) for 10 min and then XN at a final concentration of 50 μM was added, and images were taken with a confocal fluorescence microscope (Leica, Wetzlar, Germany) equipped with a temperature and CO_2-controlled microscope stage (Cyt *c* GFP ex/em: Ar 488/500–550 nm; Hoechst ex/em: diode 405/530 nm). Scans were recorded every 10 min for 1 h in total.

Generation of BPH-1 pseudo-ρ 0 (ρ^0) cells

BPH-1 ρ^0 cells were generated by addition of 250 nM ethidium bromide and 50 μg/ml uridine to RPMI 1640 cell culture medium for 8 d and a minimum of 2 passages (31). Then, cells were seeded in regular RPMI 1640 medium, and measurements of ROS production were performed as described above. To confirm depletion of mitochondria, DNA expression of "mitochondrial origin of replication" was quantified by PCR, as described previously (32).

Mitochondrial respiratory chain complex inhibition studies

Submitochondrial particles (SMPs) from bovine heart were prepared as described previously (33), and the catalytic activities of respiratory chain complexes I–IV were investigated (34). In brief, complex I activity was detected by NADH oxidation, complex II activity was detected by dichloroindophenol reduction, and complex III activity was assessed by cyt *c* reduction. Complex IV activity was measured by cyt *c* oxidation. Incubation with specific inhibitors of complexes I–III, *i.e.*, with 2-*n*-decylquinazolin-4-yl-amin (DQA), malonate, and stigmatellin, led to 80–97% ($P<0.001$) inhibition of complex activities, confirming specific enzymatic activities in our assay system.

Impact of XN on electron flux from complex I to complex III and from complex II to complex III was measured in mitochondria from BPH-1 cells. In brief, trypsinized BPH-1 cells were pelleted and lysed by 15× resuspension through a 22-gauge needle. After centrifugation (600 *g*, 10 min, 4°C), the mitochondria-containing fraction was used to measure complex activity in the presence of 6.25–50 μM XN, essentially as described previously (34), using NADH and succinate, respectively, as substrates and following cyt *c* reduction in the presence of NaCN.

Cellular ATP measurement

BPH-1 cells were seeded in cell culture-treated white 96-well plates (Greiner, Frickenhausen, Germany) and grown over-

night. Cell culture medium was changed, and cells were treated with increasing concentrations of XN and for several time intervals as indicated and washed with PBS once, and 200 μl cell culture medium containing 50% (v/v) CellTiter Glo (Promega, Madison, WI, USA), was added to each well. After 10 min of incubation at room temperature, chemiluminescence was measured using a Spectra Max $M5^E$ instrument (Molecular Devices, Sunnyvale, CA, USA). Cellular ATP levels were quantified based on an ATP standard curve in the range of 0–250 pmol/μl and normalized to protein levels.

Measurement of mitochondrial membrane potential and cyt *c* release

Mitochondrial membrane potential ($\Delta\Psi_m$) was measured using the dye JC-1 (5,5′,6,6′-tetrachloro-1,1′,3,3′-tetraethylbenzimidazolylcarbocyanine iodide). BPH-1 cells were grown overnight. Cell culture medium was changed, and cells were treated with varying concentrations of XN for several time intervals, as indicated. Cell culture medium was removed and replaced with medium containing JC-1 (1 μg/ml, diluted 1:2500 from stock prepared in DMSO) for 30 min at 37°C. After being washed once with PBS, cells were pelleted by centrifugation (600 *g* max, 5 min, 4°C). The pellet was resuspended in PBS containing 1 mM EDTA and analyzed with a FACS Calibur (photomultiplier set at ~390 V in FL1 and ~320 V in FL2, FL-1-FL2 compensation ~4.0% and FL2-FL1 compensation ~10.6%). Loss of $\Delta\Psi_m$ was quantified by quadrant analysis, with the bottom right quadrant representing cells with disrupted membrane potential (loss of red fluorescence).

Cyt *c* release was detected by Western blotting in cytosolic fractions of BPH-1 cells treated with XN for various time intervals as indicated or in a dose-dependent manner after 24 h of treatment. To generate cytosolic extracts, treated BPH-1 cells were trypsinized, pelleted, resuspended in PBS, and snap frozen in liquid nitrogen. After removal of cellular fragments by centrifugation (14,000 *g* max, 10 min, 4°C), 2.5 μg of total cytosolic protein was subjected to SDS-PAGE (15% acrylamide) under standard conditions (35). Cytosolic cyt *c* was detected using anti-cytochrome *c* antibody (Clontech, San Diego, CA, USA; diluted 1:1000 in 5% milk/TBS-T and incubated at 4°C overnight).

Cytotoxicity assay

Sulforhodamin B staining was performed as described earlier (36). To measure the influence of MnTMPyP and NAC treatment on XN-induced cytotoxicity, cells were preincubated with 50 μM MnTMPyP for 1 h before addition of XN or cotreated with 2 mM NAC.

Cell cycle distribution and Western blot analyses

Cell cycle distribution and detection of PARP cleavage by Western blotting was carried out as described previously (37). To measure protective effects of MnTMPyP on XN-induced cell cycle arrest and induction of apoptosis, cells were preincubated with 50 μM MnTMPYP for 1 h before addition of XN.

Statistical analysis

Results are presented as means ± SD. For statistical evaluation, 1 and 2-way ANOVA analysis and Tukey's HSD multiple comparison test or Student's *t* test was applied using JMP Statistical Discovery software (SAS Institute, Cary, NC, USA). Values of $P < 0.05$ were considered significant.

RESULTS

XN treatment induces formation of superoxide anion radicals

To detect prooxidative potential of XN, we utilized 2 redox-sensitive fluorescent indicators. Initial experiments with 2′,7′-dichlorodihydrofluorescein diacetate (H_2DCF-DA) revealed an immediate and dose-dependent increase in fluorescence after addition of XN to BPH-1 benign prostatic hyperplasia cells (Supplemental Fig. S1). Since H_2DCF-DA is oxidized unspecifically under conditions of "generalized oxidative stress" (38), we used DHE, which is more specifically oxidized by $O_2^{-\cdot}$, for all subsequent experiments. Cotreatment of BPH-1 cells with 12.5 μM XN and 25 μM DHE caused an immediate increase in DHE oxidation to fluorescent 2-hydroxyethidium (39), indicative of $O_2^{-\cdot}$ induction by XN. In the absence of cells, there was no increase in DHE oxidation by XN (not shown). Antimycin A, a complex III inhibitor of the mitochondrial respiratory chain, served as positive control for the induction of $O_2^{-\cdot}$, and we observed similar kinetics of DHE oxidation with both compounds at a test concentration of 12.5 μM (**Fig. 1*A***). Treatment of BPH-1 cells with XN in a concentration range of 1.6–25 μM for 10 min caused a significant dose-dependent increase in $O_2^{-\cdot}$ formation (EC_{50}±SD of maximal $O_2^{-\cdot}$ induction =4.2±0.1 μM) with a maximum 14.7-fold induction at a XN concentration of 12.5 μM ($P<0.001$; Fig. 1*B*). In contrast, addition of 50 μM H_2O_2 to BPH-1 cells did not oxidize DHE and thus confirmed the specificity of DHE for $O_2^{-\cdot}$. $O_2^{-\cdot}$ formation was not limited to the BPH-1 cell line, as similar dose-dependent effects were detected in 2 human prostate cancer cell lines, LNCaP (EC_{50}=2.9±0.2 μM) and PC-3 (EC_{50}=2.3±0.1 μM), SkBr3 human breast cancer cells (EC_{50}=4.0±0.5 μM), and RAW 264.7 murine macrophages (EC_{50}=4.0±0.3 μM; Supplemental Fig. S2). EC_{50} values obtained with the prostate cancer cell lines were significantly lower than with the benign prostatic hyperplasia cell line BPH-1 ($P<0.001$, ANOVA).

We next investigated whether $O_2^{-\cdot}$ formation was a continuous or transient effect of XN. BPH-1 cells were treated with 12.5 μM XN for 5 to 45 min and washed, and the rate of DHE oxidation was measured after addition of the dye. As indicated in Fig. 1*C*, XN-induced $O_2^{-\cdot}$ formation was a short and transient effect. We observed a maximum induction after 5 to 15 min ($P<0.001$), whereas DHE oxidation was completely diminished after 30 min of XN treatment. After 45 min, the inhibitory effect was even more pronounced (up to 2.2-fold, $P<0.001$), which may indicate antioxidant action of XN after extended incubation periods.

Next, we were interested whether XN-mediated ROS production was selective for $O_2^{-\cdot}$. Also, polyphenols have been reported to cause artifactual generation of H_2O_2 when incubated with cell culture medium (40). Therefore, we measured H_2O_2 levels in RPMI 1640 cell

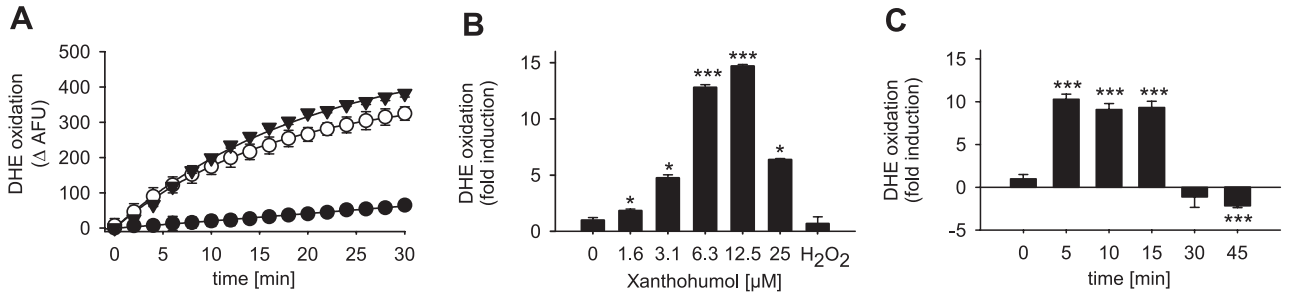

Figure 1. XN transiently induces $O_2^{-\cdot}$ in a time- and dose-dependent manner. *A*) Time-dependent increase in DHE oxidation expressed in arbitrary fluorescence units (AFU) in BPH-1 cells, indicative of $O_2^{-\cdot}$ formation after XN treatment. Antimycin A (complex III inhibitor) served as positive control for $O_2^{-\cdot}$ formation. Control (●), 12.5 μM XN (○), and 12.5 μM antimycin A (▼) are shown. *B*) Dose-dependent increase in $O_2^{-\cdot}$ formation after 10 min of treatment with XN. H_2O_2 (50 μM) served as negative control. Data are expressed as a fold increase in DHE oxidation rate in relation to solvent control. *C*) Transient $O_2^{-\cdot}$ induction after XN treatment, measured by DHE oxidation after 20 min. Cells were pretreated with XN at a concentration of 12.5 μM for times indicated and washed before DHE addition. Data are expressed as fold induction realative to solvent control. Data are means ± SD ($n = 3$). $^*P < 0.05$, $^{***}P < 0.001$; 1-way ANOVA.

culture medium after addition of XN under cell-free conditions and in the presence of BPH-1 cells, using the Amplex Red assay (Invitrogen). Under both conditions, XN at concentrations up to 50 μM did not cause any H_2O_2 formation. In contrast, after incubation of RPMI with (−)-epigallocatechin-3-gallate used as a positive control at concentrations from 1.6 to 50μM, a dose-dependent increase in H_2O_2 levels from 0.75 ± 0.03 to 39.2 ± 0.83 μM was detected.

XN-induced $O_2^{-\cdot}$ formation is inhibited by antioxidant treatment

To further confirm that DHE oxidation was mediated by $O_2^{-\cdot}$ induced by XN, we cotreated BPH-1 cells with 10 μM XN and ascorbic acid (AA) or NAC at mM concentrations. Both AA and NAC inhibited XN-induced $O_2^{-\cdot}$ formation significantly in a dose-dependent manner ($P<0.001$ at the 2 highest concentrations), with IC_{50} values of 5.1 ± 0.1 and 0.8 ± 0.2 mM, respectively (**Fig. 2*A*, *B***). Pretreatment of BPH-1 cells with the cell permeable superoxide dismutase (SOD)-mimetic MnTMPyP [manganese (III) tetrakis(1-methyl-4-pyridyl)porphyrin] in a concentration range of 1.6–50 μM for 1 h before induction of $O_2^{-\cdot}$ by addition of 10 μM XN also significantly reduced DHE oxidation ($P<0.001$ at 50 μM MnTMPyP), and we determined an IC_{50} value of 7.0 ± 2.2 μM (Fig. 2*C*).

XN-induced $O_2^{-\cdot}$ formation leads to thiol oxidation and depletion

Glutathione (GSH) constitutes the major intracellular antioxidant defense against ROS and has been shown to scavenge $O_2^{-\cdot}$ and other ROS by oxidation to thiyl radical and further oxidation to GSSG (41). Therefore, we determined changes in intracellular thiol-disulfide levels as a consequence of XN treatment using GSH and GSSG as standards. BPH-1 cells were treated with increasing XN concentrations, and after 6 h total thiol levels were determined. Increasing XN concentrations caused a significant ($P<0.001$ at 25 and 50 μM) dose-dependent depletion of total thiols of 17–62%, and we calculated an IC_{50} value of 24.3 ± 11 μM (**Fig. 3*A***). To test whether XN-induced $O_2^{-\cdot}$ formation would cause oxidation of GSH to GSSG, BPH-1 cells were treated with 50 μM XN, and after incubation for 0.5–6 h, oxidized and reduced thiol levels were measured. As early as 30 min after addition of XN, GSSG levels were significantly elevated by 15% compared with solvent controls cells ($P<0.001$), and this increase remained constant up to 6 h after XN treatment (Fig. 3*B*). In

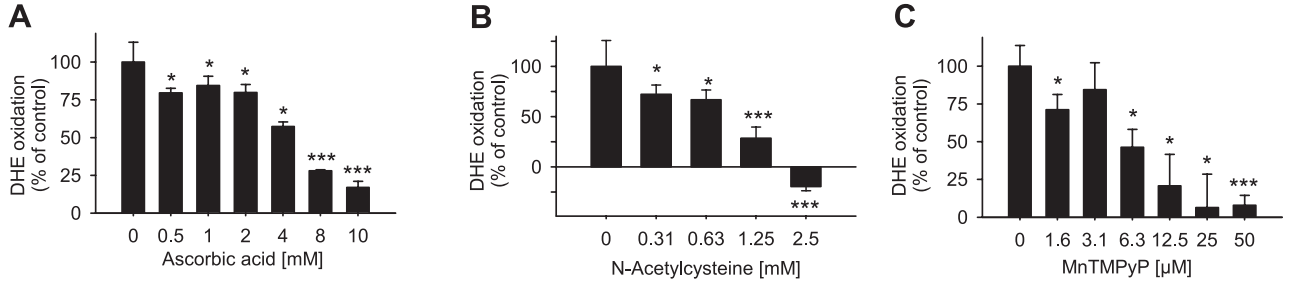

Figure 2. Inhibition of XN-induced $O_2^{-\cdot}$ formation. BPH-1 cells were stimulated with XN at a concentration of 10 μM for 10 min to induce $O_2^{-\cdot}$, detected by DHE oxidation. Dose-dependent reduction in DHE oxidation by cotreatment with the antioxidants ascorbic acid (*A*) and NAC (*B*) and by 1 h pretreatment with the SOD mimetic MnTMPyP (*C*) in comparison with XN-treated control (set as 100%). Data are means ± SD (n=3). $^*P < 0.05$, $^{***}P < 0.001$; 1-way ANOVA.

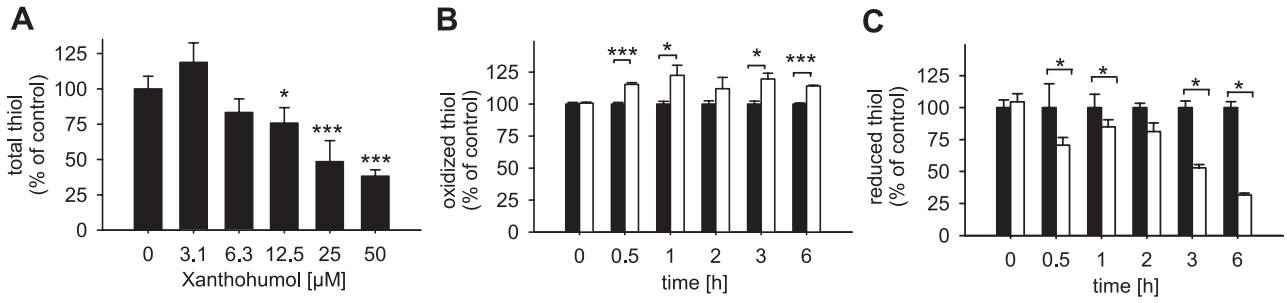

Figure 3. XN-mediated thiol oxidation and depletion. *A*) Dose-dependent oxidation of total thiol levels after 6 h of XN treatment in BPH-1 cells. *B, C*) Time-dependent thiol oxidation (*B*) and depletion of reduced thiol levels (*C*) in BPH-1 cells, treated with XN at a concentration of 50 μM (open bars) compared with solvent controls (solid bars). Control levels of reduced and oxidized thiols were in the range of 199–222 and 2.8–3.4 nmol/mg protein, respectively. Data are means ± SD (n=3). *$P<$ 0.05, ***$P<$ 0.001; 1-way ANOVA.

parallel, reduced thiol levels were significantly depleted by XN treatment in a time-dependent manner with 68% reduction after 6 h ($P<0.05$; Fig. 3*C*). Alternatively, increased GSSG levels may be due to XN oxidation by intracellular oxidases and peroxidases in the presence of GSH or NADH and catalytic amounts of H_2O_2, as suggested by Galati *et al.* (42) (Supplemental Fig. S3).

XN-induced $O_2^{-\cdot}$ formation is of mitochondrial origin

Fluorescence microscopy after staining of BPH-1 cells with the mitochondrial superoxide indicator MitoSOX Red gave a first indication that mitochondria might be the source of XN-induced $O_2^{-\cdot}$ (not shown). Consequently, we isolated mitochondria from murine liver to measure $O_2^{-\cdot}$-induction by XN. Mitochondria (0.3 mg/ml) were suspended in PBS containing 25 μM DHE and then treated with XN and antimycin A, respectively, in a concentration range of 1.6–25 μM. Similar to the results obtained with intact cells, both compounds caused an immediate, dose-dependent increase in DHE oxidation (EC_{50}=11.4±1.8 and 12.4±0.9 μM, respectively), indicating that mitochondria were indeed targeted by XN (**Fig. 4*A***).

This observation was further investigated using MCF-7 cells stably transfected with GFP-labeled cytochrome *c* (cyt *c* GFP; ref. 43). Under nonapoptotic conditions, cyt *c* is mainly localized in mitochondria and was used as a mitochondrial marker. Cyt *c* GFP cells were treated with 25 μM XN for 10 min, then washed once with PBS, and incubated with 5 μM MitoSOX Red for 5 min. Confocal fluorescence microscopy images revealed brightly red fluorescing mitochondria in cyt *c* GFP cells treated with XN, indicative of mitochondrial $O_2^{-\cdot}$ generation, which was much less pronounced in solvent-treated control cells (Fig. 4*B*). Overlay of green and red fluorescence confirmed the mitochondrial origin of XN-induced $O_2^{-\cdot}$. Interestingly, pretreatment of cyt *c* GFP cells with 50 μM MnTMPyP for 1 h almost completely eliminated oxidation of MitoSOX Red by mitochondrial $O_2^{-\cdot}$ induced by XN.

We also generated BPH-1 ρ^0 cells, which lack mitochondrial DNA, resulting in nonfunctional mitochondria. BPH-1 ρ^0 cells were treated with XN at concentrations up to 25 μM in the presence of 25 μM DHE. Whereas in fully functional BPH-1 cells incubation with 25 μM XN for 10 min resulted in a 8.7-fold induction of $O_2^{-\cdot}$ formation, DHE oxidation was significantly reduced by 86% ($P<0.05$) in BPH-1 ρ^0 cells ($EC_{50}>25$ μM), further indicating that intact mitochondria are a prerequisite for XN-mediated $O_2^{-\cdot}$ induction (Fig. 4*C*). Reduction in functional mitochondria in BPH-1 ρ^0 cells was confirmed by PCR amplification of origin of replication of mitochondrial heavy strand DNA (Fig. 4*D*). Further, BPH-1 ρ^0 showed reduced respiratory activity, compared with normal BPH-1 cells, confirming a lack of intact mitochondria (not shown).

XN inhibits complexes I-III of the respiratory chain and depletes ATP

Inhibition of mitochondrial respiration leads to an increased release of $O_2^{-\cdot}$, as indicated by the results obtained with the complex III inhibitor antimycin A (Figs. 1*A* and 4*A*). Therefore, we were wondering whether mitochondrial respiration was a target of XN action. We monitored oxygen consumption of isolated mouse liver mitochondria using a Clark-type oxygen electrode (Hansatech, Norfolk, England). After addition of 100 μM ADP, oxygen consumption was increased, indicating active, electron absorbing complex V activity (ATPase). This respiratory state was significantly inhibited by the addition of both XN and antimycin A at a concentration of 100 μM ($P<0.05$; Supplemental Figure S4).

We next performed detailed complex inhibition studies with SMPs isolated from bovine heart. As depicted in **Table 1**, XN had to be tested at relatively high concentrations from 50 to 200 μM to achieve inhibition of the individual complexes I, II, and III, owing to the high abundance of respiratory chain proteins in SMPs. NADH:ubiquinone oxidoreductase (complex I) activity, succinate dehydrogenase (complex II) activity, as well as complex III activity (cytochrome bc_1 complex) were significantly inhibited by XN at concentrations >100 μM ($P<0.05$), whereas cytochrome *c* oxidase

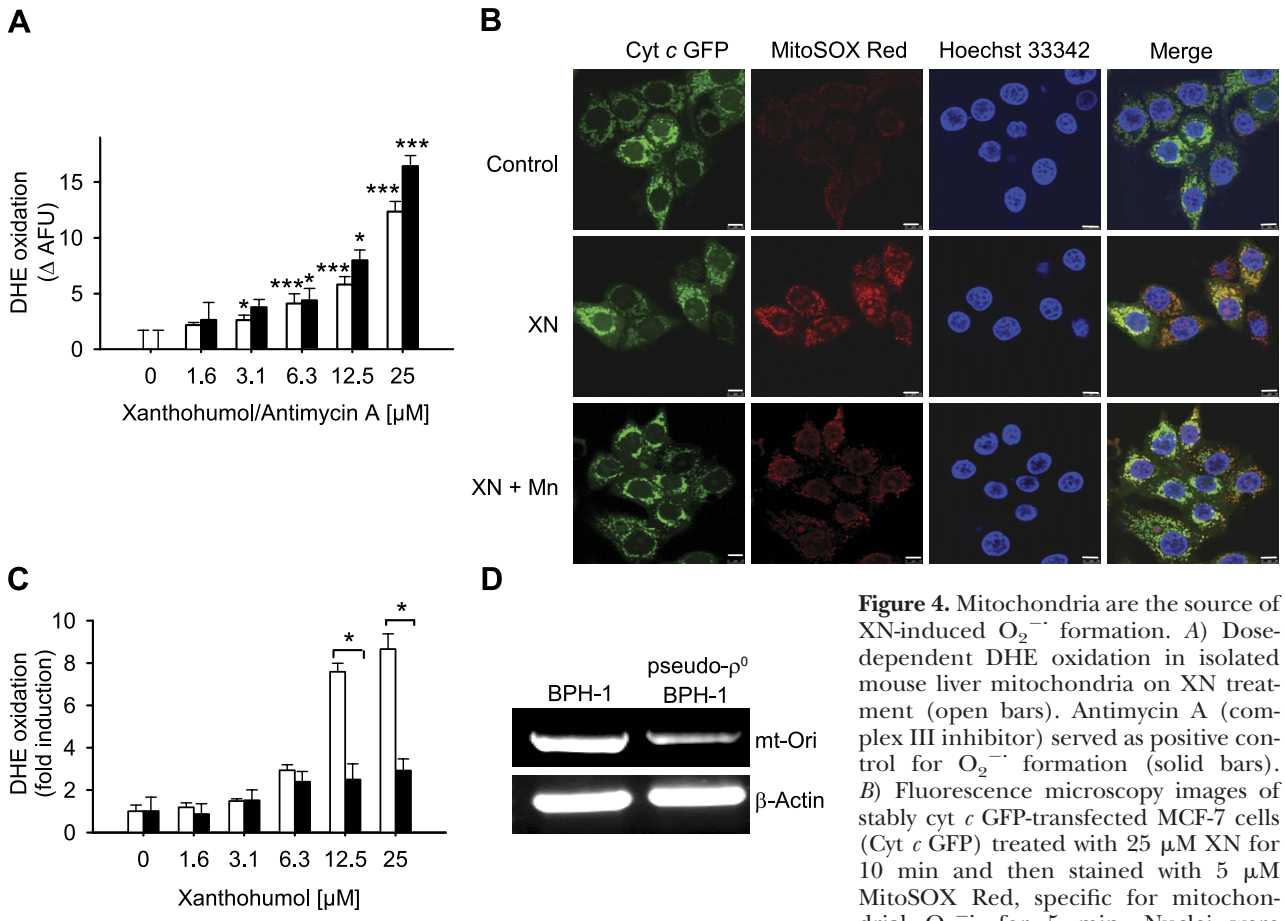

Figure 4. Mitochondria are the source of XN-induced $O_2^{-\cdot}$ formation. *A*) Dose-dependent DHE oxidation in isolated mouse liver mitochondria on XN treatment (open bars). Antimycin A (complex III inhibitor) served as positive control for $O_2^{-\cdot}$ formation (solid bars). *B*) Fluorescence microscopy images of stably cyt *c* GFP-transfected MCF-7 cells (Cyt *c* GFP) treated with 25 μM XN for 10 min and then stained with 5 μM MitoSOX Red, specific for mitochondrial $O_2^{-\cdot}$, for 5 min. Nuclei were stained with 1 μg/ml Hoechst 33342. Overlay indicates mitochondrial origin of XN-induced $O_2^{-\cdot}$. Pretreatment with the SOD-mimetic MnTMPyP (Mn) at a concentration of 50 μM for 1 h prevented XN-mediated mitochondrial $O_2^{-\cdot}$ formation (bottom panel). Scale bar = 10 μm. *C*) Reduced $O_2^{-\cdot}$ formation, measured by DHE oxidation after 10 min of incubation, on XN treatment in BPH-1 ρ^0 cells, harboring nonfunctional mitochondria (solid bars), compared with normal BPH-1 cells (open bars). *D*) PCR amplification of the origin of replication of mitochondrial heavy strand DNA [origin of replication of mitochondrial heavy strand DNA (mt-Ori)], demonstrating depletion of mtDNA. β-Actin served as loading control. Data are means ± SD (n=3). *$P < 0.05$, ***$P < 0.001$; 1-way ANOVA.

(complex IV) activity detected by cyt *c* oxidation was not affected by XN (data not shown). Overall, XN-mediated inhibition of individual complexes of the respiratory chain appeared to be unspecific, and we cannot exclude that it may be due to protein binding or complexation with iron. Accordingly, we could demonstrate *in vitro* chelation of XN with Fe^{2+}, Fe^{3+}, and hemin by UV/VIS spectrophotometry (Supplemental Fig. S5).

TABLE 1. *Summary of XN-mediated inhibition of complexes I–III of the mitochondrial respiratory chain, measured in bovine heart SMPs*

XN concentration (μM)	Percentage activity		
	Complex I	Complex II	Complex III
50	107.8 ± 5.7	98.1 ± 1.2	87.2 ± 3.5
75	98.9 ± 5.1	92.4 ± 2.0*	83.9 ± 6.6†
100	77.7 ± 3.9*	85.2 ± 1.9*	83.1 ± 3.2*
200	41.1 ± 9.0*	62.9 ± 3.8*	47.9 ± 10.1*

Data are means ± SD. *$P < 0.05$, †$P = 0.06$; ANOVA, Tukey-Kramer HSD test.

To better mimic conditions of cellular $O_2^{-\cdot}$ formation by XN, crude mitochondrial extracts prepared from BPH-1 cells were treated with 6.25–50 μM XN and the impact of XN on the electron flux from complex I to complex III and complex II to complex III was measured. Under these conditions, XN treatment significantly (P<0.001 at 50 μM) inhibited electron flux from complex I to complex III by 13–72% (IC_{50}=28.1±2.4 μM; **Fig. 5*A***). The electron flux from complex II to complex III was also dose-dependently inhibited by 38–71% by XN (IC_{50}=24.4±5.2 μM; Fig. 5*B*).

The mitochondrial respiratory chain is coupled to the production of ATP. Interestingly, treatment of BPH-1 cells with XN at a concentration of 12.5 μM for up to 2 h caused a significant 11–25% depletion of ATP (P<0.05), whereas treatment with 50 μM XN for 5 and 15 min resulted in a 78 and 95% decrease in cellular ATP levels and complete depletion after 30 and 60 min (P<0.05; **Fig. 6*A***). When BPH-1 cells were incubated with XN at concentrations of 3.1–50 μM for 15 min,

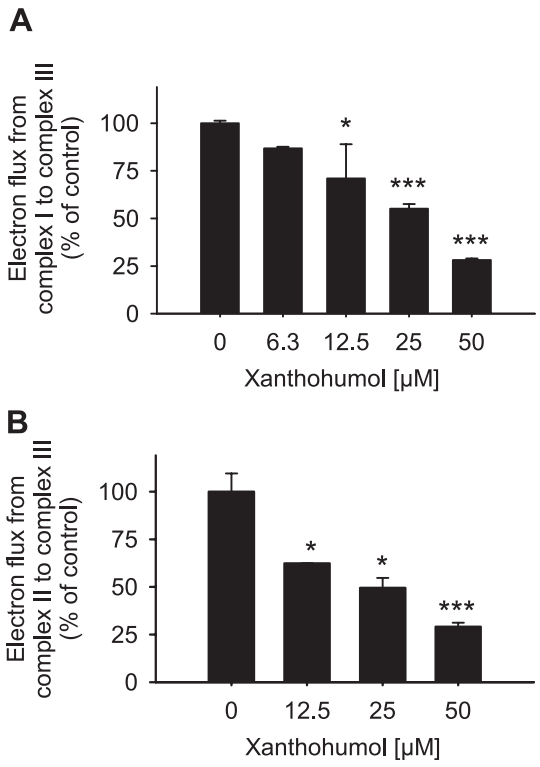

Figure 5. XN inhibits electron flux in mitochondria isolated from BPH-1 cells. *A*) Electron flux from complex I to complex III. Change in absorption at 550 nm was measured, indicating cyt *c* reduction at complex III after addition of NADH, the substrate for complex I. *B*) Electron flux from complex II to complex III. Change in absorption at 550 nm was measured, indicating cyt *c* reduction at complex III after addition of succinate, the substrate for complex II. Data are means ± SD (n=3). *$P < 0.05$, ***$P < 0.001$; 1-way ANOVA.

ATP levels were dose dependently decreased by 8–88% (IC_{50}=26.7±3.7 μM; Fig. 6*B*).

XN causes a breakdown of the mitochondrial membrane potential and cyt *c* release

Mitochondria play a central role in apoptosis induction (44). Mitochondrial outer membrane permeabilization and disruption of the mitochondrial membrane potential are irreversible triggers of the mitochondrial cell death cascade leading to cytochrome *c* release from the intermembrane space of the mitochondria into the cytosol. The mitochondrial membrane potential $\Delta\Psi_m$ as a crucial indicator of mitochondrial integrity can be assessed by staining with the fluorescent indicator dye JC-1. Treatment of BPH-1 cells with XN at a concentration of 25 μM caused a rapid depolarization of $\Delta\Psi_m$, depicted by representative dot blots in **Fig. 7*A***. Cells with low red fluorescence (bottom right quadrant) increased from 8–67.8% within 10 min and further increased to 69.9% within 30 min. The mitochondrial uncoupler carbonyl cyanide 3-chlorophenylhydrazone (CCCP) was used as a positive control. Treatment of BPH-1 cells with XN in a concentration range of 3.1–50 μM led to a significant dose-dependent breakdown of $\Delta\Psi_m$, as indicated in Fig. 7*B* (P<0.05, 2-way ANOVA). This effect was significantly inhibited by 35–61% by pretreatment with 50 μM MnTMPyP for 1 h (P<0.001, 2-way ANOVA).

Usually the opening of the outer mitochondrial membrane is accompanied by the release of cyt *c* into the cytosol. Therefore, we assessed the effects of XN on cyt *c* release from mitochondria using confocal microscopy live cell imaging with GFP cyt *c* labeled MCF-7. Cells were treated with 50 μM of XN, and images were taken immediately after the addition of XN and every 10 min for 60 min. As early as 10 min after XN treatment, we observed changes in mitochondrial cyt *c* organization (Fig. 7*C*, center panel), which were more pronounced after 30 min of treatment and did not appear in DMSO-treated control cells (Fig. 7*C*, top panel). After 1 h of XN treatment, fluorescing cyt *c* GFP molecules were no longer detectable in mitochondria. Again, pretreatment with 50 μM MnTMPyP for 1 h almost completely abrogated XN-mediated effects on cyt *c* release (Fig. 7*C*, bottom panel).

In parallel, Western blots of cytosolic protein fractions of BPH-1 cells treated with 25 μM XN demonstrated a time-dependent release of cyt *c* into the cytosol. Elevated cytosolic cyt *c* levels were detectable already 30 min after addition of XN and further increased until 24 h of incubation (Fig. 7*D*). After 24 h, a dose-dependent cyt *c* release was confirmed with

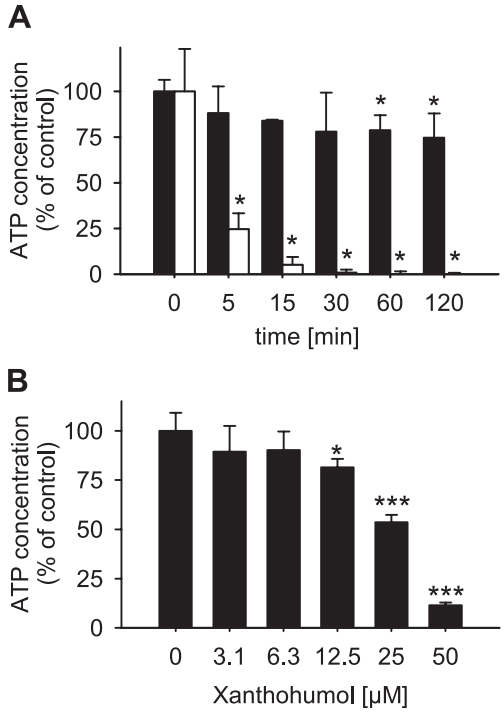

Figure 6. XN depletes intracellular ATP levels. *A*) Time-dependent ATP depletion in BPH-1 cells, treated with 12.5 (solid bars) and 50 μM XN (open bars). *B*) Dose-dependent reduction in ATP levels after 15 min of XN treatment. Values were normalized to an ATP standard curve. ATP concentrations of untreated controls were in a range of 27–45 pmol/mg protein. Data are means ± SD (n=3). *$P < 0.05$, *** $P < 0.001$; 1-way ANOVA.

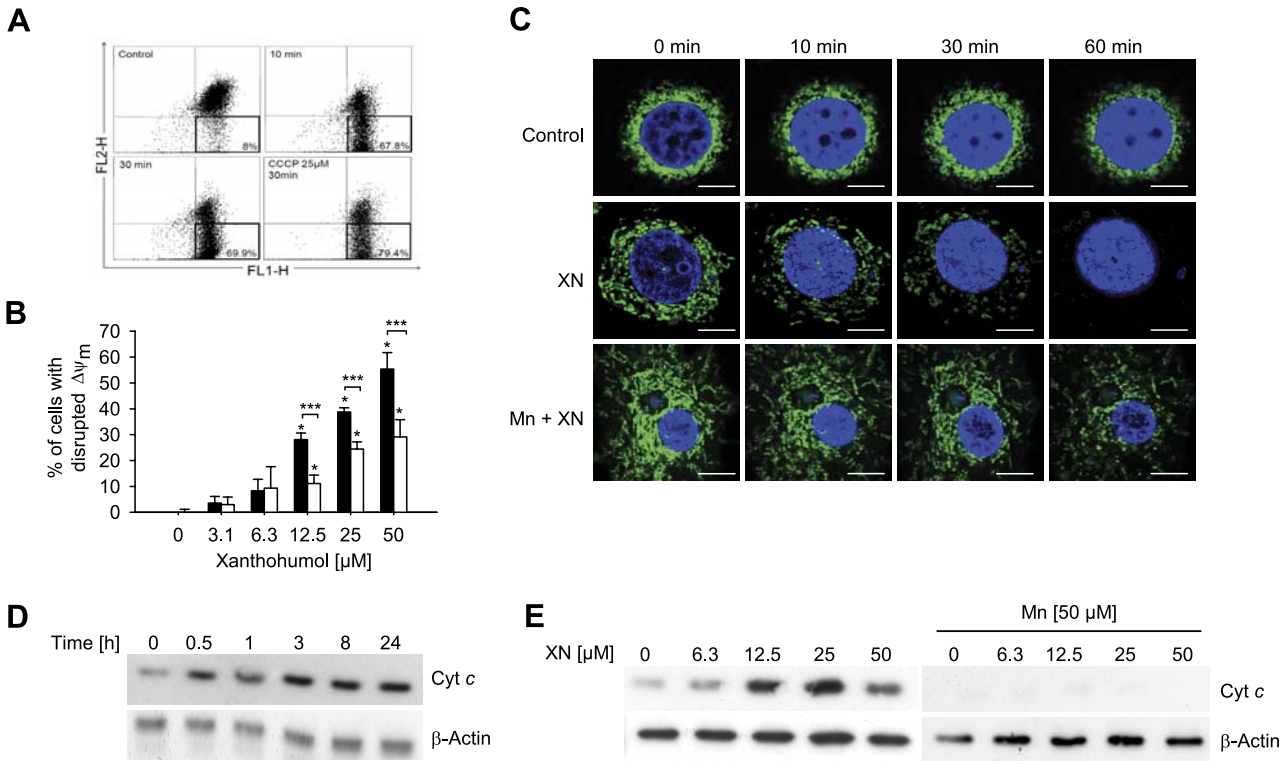

Figure 7. XN treatment impairs mitochondrial functions. *A*) Time-dependent breakdown of mitochondrial membrane potential ($\Delta\Psi_m$) in BPH-1 cells, after treatment with 25 μM XN for 10 and 30 min or 25 μM CCCP for 30 min as indicated, measured by FACS analysis after staining with the fluorescent dye JC-1. FL1, green fluorescence; FL2, red fluorescence. Highlighted quadrants indicate percentage of cells with disrupted $\Delta\Psi_m$. *B*) Dose-dependent increase in percentage of BPH-1 cells with disrupted $\Delta\Psi_m$ after 30 min of XN treatment (solid bars). Pretreatment with 50 μM MnTMPyP for 1 h (open bars) reduced XN-induced breakdown of $\Delta\Psi_m$ ($P<0.001$). Data are means ± SD (n≥3). $^*P < 0.05$, $^{***}P < 0.001$, 2-way ANOVA. Dose-dependent increase in disrupted $\Delta\Psi_m$ was compared separately for both treatments with solvent control. Also, interaction of both treatments was compared. *C–E*) XN treatment disrupts mitochondria and causes cyt *c* release. *C*) Live-cell imaging of cyt *c* GFP-transfected MCF-7 cells during incubation with 50 μM XN as indicated and after pretreatment with 50 μM MnTMPyP for 1 h. Nuclei were stained with 1 μg/ml Hoechst 33342. *D*) Time-dependent cytosolic accumulation of cyt *c* in BPH-1 cells treated with 25 μM XN for indicated times. Scale bar = 10 μm. *E*) Cytosolic cyt *c* detection after 24 h of incubation with XN in a concentration range of 0–50 μM (left panel) and prevention by pretreatment with 50 μM MnTMPyP for 1 h (right panel). β-Actin served as loading control.

increasing XN concentrations in a range of 6.3–50 μM. Pretreatment of BPH-1 cells with 50 μM MnTMPyP for 1 h completely prevented XN-induced cyt *c* release to the cytosol (Fig. 7*E*).

Antiproliferative effects and apoptosis induction are reduced by MnTMPyP

XN has been shown to possess antiproliferative activity and to induce apoptosis *via* down-regulation of Bcl-2 protein expression; activation of caspases-3, -7, -8, and 9; and PARP cleavage (22). To test whether these mechanisms are initiated by the immediate induction of $O_2^{-\cdot}$ formation by XN, BPH-1 cells were either pretreated with 50 μM MnTMPyP for 1 h or cotreated with 2 mM NAC and XN in a concentration range of 0.4–50 μM for 72 h before cell growth was determined by sulforhodamine B staining. Both cotreatment with NAC and pretreatment with MnTMPyP significantly reduced XN-mediated cytotoxicity. The IC_{50} value for BPH-1 treatment with XN was 6.7 ± 0.2 μM. NAC cotreatment resulted in a 2-fold higher IC_{50} of 12.2 ± 0.13 μM ($P<0.001$, ANOVA), whereas MnTMPyP pretreatment increased the IC_{50} of XN almost 6-fold to 41.4 ± 7.6 μM ($P=0.001$, ANOVA; **Fig. 8*A***). These results demonstrate that induction of $O_2^{-\cdot}$ by XN is the initial trigger for antiproliferative activity, since scavenging of $O_2^{-\cdot}$ by antioxidants or dismutation to H_2O_2 by the SOD mimetic abrogated XN-mediated cytotoxicity.

To further investigate whether XN-induced $O_2^{-\cdot}$ formation is also involved in apoptosis induction, we assessed PARP cleavage by Western blotting. When BPH-1 cells were incubated with XN at concentrations of 10–40 μM for 48 h, a dose-dependent increase in the cleaved fragment of PARP was detected. PARP cleavage was fully inhibited by pretreatment for 1 h with 50 μM MnTMPyP, indicating that $O_2^{-\cdot}$ induction indeed initiates the induction of apoptosis by XN (Fig. 8*B*). To verify this observation, cell cycle distribution of BPH-1 cells treated with XN for 72 h was compared with cells pretreated with 50 μM MnTMPyP for 1 h before XN

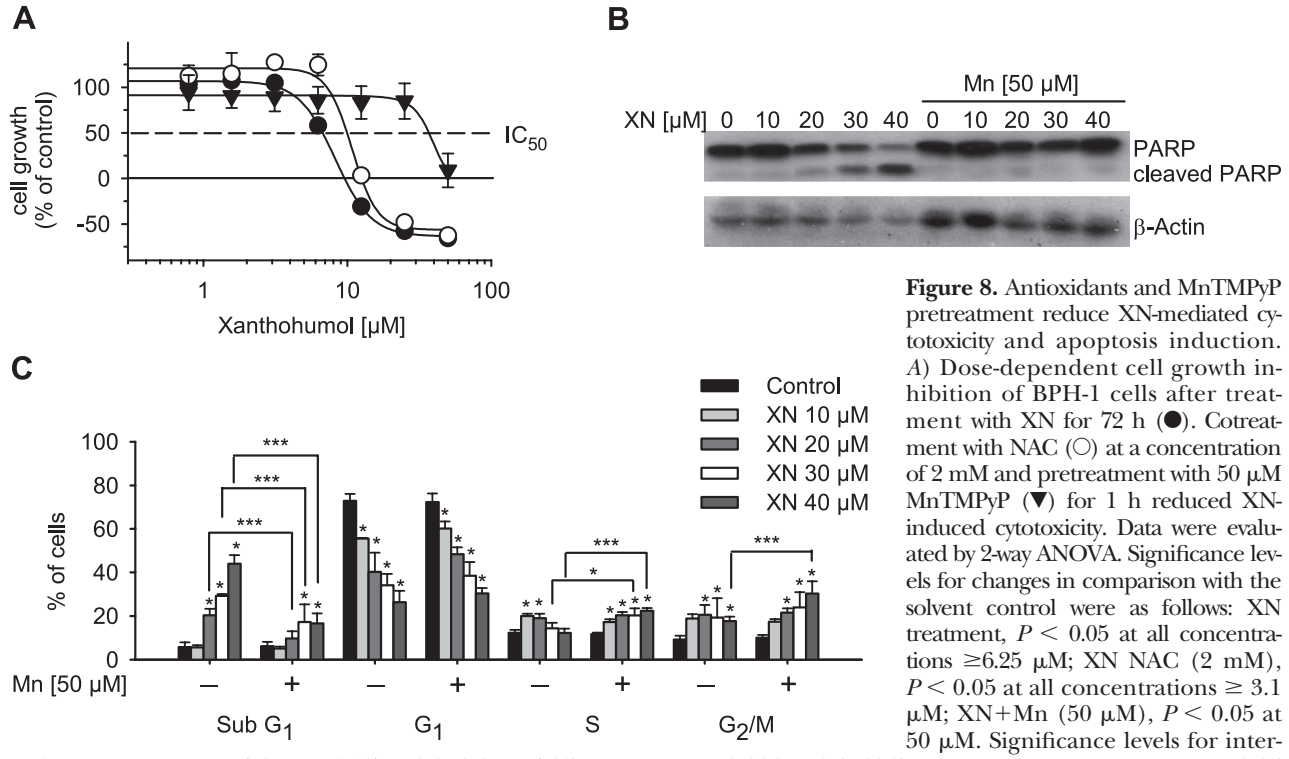

Figure 8. Antioxidants and MnTMPyP pretreatment reduce XN-mediated cytotoxicity and apoptosis induction. *A*) Dose-dependent cell growth inhibition of BPH-1 cells after treatment with XN for 72 h (●). Cotreatment with NAC (○) at a concentration of 2 mM and pretreatment with 50 μM MnTMPyP (▼) for 1 h reduced XN-induced cytotoxicity. Data were evaluated by 2-way ANOVA. Significance levels for changes in comparison with the solvent control were as follows: XN treatment, $P < 0.05$ at all concentrations ≥6.25 μM; XN NAC (2 mM), $P < 0.05$ at all concentrations ≥ 3.1 μM; XN+Mn (50 μM), $P < 0.05$ at 50 μM. Significance levels for interaction: XN *vs.* XN+NAC, $P < 0.05$ at 0.8, 1.6, and 25 μM XN, $P < 0.001$ at 3.1–12.5 μM XN; XN *vs.* XN+Mn, $P < 0.05$ at 0.8–3.1 μM XN, $P < 0.001$ at 6.25–50 μM XN. Asterisks to indicate significance levels were omitted for clarity. *B*) Representative Western blot images of PARP cleavage as an indicator of apoptosis induction in BPH-1 after incubation with XN as indicated for 48 h (left) and inhibition by 1 h pretreatment with MnTMPyP (right). β-Actin served as loading control. *C*) FACS analysis of cell cycle distribution of BPH-1 cells treated for 48 h with XN as indicated (−) and after 1 h pretreatment with 50 μM MnTMPyP (+). Data are means ± SD ($n = 3$). *$P < 0.05$, ***$P < 0.001$; 2-way ANOVA. Asterisks above bars indicate significance levels compared with solvent controls; asterisks above brackets indicate significant changes between XN and pretreatment with MnTMPyP.

addition. As indicated in Fig. 8*C*, with increasing XN concentrations, 5–44% of the cells were accumulated in the sub-G_1 cell fraction, indicative of apoptosis ($P<0.05$, 2-way ANOVA). The portion of apoptotic cells was significantly reduced by 53–63% by pretreatment with MnTMPyP ($P<0.001$, 2-way ANOVA). Under these conditions, XN at the highest concentrations resulted in S and G_2/M arrest (S-phase arrest, $P<0.05$ at 30 μM XN; both S and G_2/M arrest, $P<0.001$ at 40 μM XN, 2-way ANOVA).

DISCUSSION

Based on a previous observation that induction of apoptosis and differentiation of preadipocytes by XN have been linked to the induction of ROS (23, 24), the aim of the present study was to elucidate the kinetics, source, and downstream events of XN-induced ROS formation.

ROS are important regulators of apoptosis (2), either by directly activating apoptosis *via* mitochondria or as a consequence of mitochondria-mediated induction of apoptosis (45). In the present study, we demonstrated that XN very rapidly induces $O_2^{-\cdot}$ and that mitochondria are the source of this increase. Complex inhibition studies in submitochondrial particles and in mitochondria from BPH-1 cells revealed the inhibitory potential of XN at complexes I to III of the respiratory chain. Subsequent damage of mitochondrial integrity led to the loss of mitochondrial membrane potential, depletion of ATP, release of cyt *c*, and induction of apoptosis, detectable by PARP cleavage and an increase in the sub-G_1 fraction by flow cytometry. Importantly, we prevented almost all of these steps by pre- or cotreatment with an SOD mimetic or antioxidants, indicating that $O_2^{-\cdot}$ induction is indeed the trigger for cell death.

After having established this relationship, we were interested in the molecular mechanisms that may contribute to the immediate mitochondrial $O_2^{-\cdot}$ production induced by XN. The major function of mitochondria is to carry out oxidative phosphorylation to produce ATP. Inhibition of complexes I and III has been shown to result in rapid, excessive $O_2^{-\cdot}$ formation (46). We demonstrated inhibitory effects of XN at complexes I to III and on electron flux between complex I or II and III, which might derive from direct interaction of XN with the respective enzymes. Iron-binding properties are typical features of polyphenols (47, 48). Interestingly, incubation of XN with Fe^{2+} and Fe^{3+} ions, as well as with the Fe^{2+}-porphyrin complex hemin, resulted in dose-dependent interactions with XN (Supplemental Fig. S5). Based on these data, we speculate that XN may bind to iron atoms and thereby

inhibit iron-sulfur-complexes of respiratory chain proteins. Moreover, specific binding of XN to intracellular proteins has been demonstrated earlier (49). Recent work (50) also suggested XN-thiol adduct formation in a Michael-type addition reaction as a consequence of XN oxidation *in vitro*. These findings provide another potential mechanism of how XN interacts with enzymes of the respiratory chain and thus alters mitochondrial respiration.

Excessive $O_2^{-\cdot}$ formation has been related to a breakdown of the mitochondrial membrane potential and uncoupling of respiration (46, 51). Many phenolic compounds, such as the dietary curcumin and its derivatives, but also classical uncouplers such as CCCP or 2,4-dinitrophenol induce mitochondrial uncoupling and mitochondrial permeability transition pore (MPTP) opening, resulting in the collapse of the mitochondrial membrane potential (52, 53). XN-induced $O_2^{-\cdot}$ formation was accompanied by an immediate breakdown of the mitochondrial membrane potential. In contrast to other phenolic compounds, XN lacks uncoupling activity, despite the fact that XN contains several acidic dissociable groups that could induce uncoupling (54). XN did not induce mitochondrial swelling (data not shown), which is an indicator of MPTP opening (53). Nevertheless, XN treatment caused thiol group oxidation in isolated mitochondria (Supplemental Fig. S6), which is, beside increased ROS production and a low mitochondrial membrane potential, believed to be one of the triggers for MPTP opening (11). As a consequence of MPTP opening, the release of proapoptotic factors and subsequent apoptosis are induced (55).

Apoptosis is an energy-dependent process, and a rapid loss of ATP is normally linked to necrotic cell death (56). XN treatment significantly depleted intracellular ATP levels in a dose-dependent manner. XN at a concentration of 12.5 μM, which induced the highest $O_2^{-\cdot}$ formation, caused a 25% depletion of ATP, most likely as a direct consequence of disrupted mitochondrial respiration. In contrast, higher XN concentrations led to a very rapid drop in ATP concentration of up to 95% after 15 min already. However, no signs of necrosis were measured by PI exclusion at concentrations up to 50 μM used in the present study after 72 h of XN treatment (data not shown). In contrast, XN treatment rapidly induced the release of cyt *c* from mitochondria into the cytosol, which is one of the initial and irreversible steps of apoptosis induction. Previous studies showed down-regulation of antiapoptotic Bcl-2 expression and activation of caspases-3, -7, -8, and -9 by XN (22). Strikingly, in the present study, downstream events of apoptotic cell death, such as PARP cleavage and accumulation of cells in the sub-G_1 phase of the cell cycle were detected after 48 h of treatment only, whereas cyt *c* release was observed as early as 30 min after XN treatment. Unpublished data from our laboratory have recently indicated that XN induces autophagy, representing a mechanism of cell survival at times of stress (56, 57). Autophagy often occurs when cells are not able to maintain ATP levels or when mitochondria are damaged (58). Inhibitors of the respiratory chain have been identified before as inducers of autophagy, with $O_2^{-\cdot}$ being the major regulator (59, 60). Prolonged autophagy can result in the induction of cell death (59), and this may explain why induction of apoptosis by XN-induced $O_2^{-\cdot}$ formation as an initial trigger is delayed. Interestingly, antioxidant treatment prevented XN-induced autophagy (unpublished results). However, the detailed mechanism of XN-induced autophagy and its relation to apoptosis need to be further investigated.

As a sign of intracellular oxidative stress, we detected elevated GSSG levels and total thiol depletion on XN treatment. An unbalanced redox environment is an important regulator of progression to apoptosis (61). Accordingly, the action of various cytotoxic agents has been linked to induction of oxidative stress, depletion of intracellular GSH, and consequent apoptosis induction (62, 63). Induction of mitochondria-derived ROS was identified as an apoptotic stimulus acting *via* GSH oxidation and depletion, oxidative protein modifications, activation of caspases, and downregulation of antiapoptotic signaling molecules (41).

By now it is well accepted that many pathologies are associated with increased levels of ROS, which promote abnormal proliferation and imbalanced redox homeostasis (64, 65). It is believed that cancer cells display an aberrant redox balance and altered stress adaption compared with normal cells. Elevated levels of ROS concomitant with elevated expression of the intracellular antioxidant system have been described in cancer cells *in vitro* as well as *in vivo*. These changes might be initiated either by the expression of oncogenes, such as c-*myc* and Ras, which were found to cause ROS induction, and/or by down-regulation of tumor suppressor genes (*e.g.*, TP53), altered metabolism, and mitochondrial functions (15). Persistent oxidative stress makes affected cells more sensitive to prooxidant exposure, leading to destabilization of mitochondria and the induction of apoptosis (26, 66). On the contrary, normal cells with basal ROS levels are affected by oxidative stress to a lower extent (67). Consequently, mitochondria have emerged recently as effective targets for cancer therapeutic drugs, referred to as "mitocans" (for mitochondria and cancer; ref. 66). Distinct targets of mitocans have been identified, including but not limited to voltage-dependent anion channels, the complexes of the respiratory chain, antiapoptotic proteins Bcl-2 and Bcl-x_L, and other mitochondrial membrane bound enzymes (26). One key mechanism of mitocans involves the generation of ROS of mitochondrial origin, which are believed to mediate mitochondrial oxidation processes, which then trigger the induction of apoptosis (26). XN induces the rapid formation of $O_2^{-\cdot}$, which is of mitochondrial origin in various human cancer cell lines. As demonstrated in the present study, the effective XN concentration of half maximal $O_2^{-\cdot}$ induction was significantly higher in the benign prostatic hyperplasia cell line BPH-1 (EC_{50}=4.3±0.1 μM) than in the malignant prostate cancer cell lines

LNCaP (EC_{50}=3.0±0.2 μM) and PC-3 (EC_{50}=2.3±0.1 μM; $P<0.001$, ANOVA), indicating that with increasing malignancy cancer cell lines may indeed be more sensitive to XN-mediated $O_2^{-\cdot}$ formation. Recent studies (68) demonstrated selective killing of transformed cancer cells by dietary polyphenols *via* a ROS-mediated mechanism in ovarian epithelial cells as well as in an *in vivo* xenograft model. This implicates novel therapeutic benefits by dietary supplementation with polyphenols.

An initial safety study (69) in rats revealed no severe toxic side effects of XN when it was applied orally at doses of 10 and 100 mg/kg body wt/d for extended periods of time. Peak plasma concentrations after a single application of 1000 mg XN/kg body wt to female Sprague-Dawley rats were detected 4 h after oral application. The XN-4′-*O*-glucuronide was identified as the major metabolite, with a maximal concentration of 3.1 μM. Unmetabolized XN was detectable with a maximal concentration of 0.34 μM 4 h after administration (20). Different routes of applications and improved formulations (currently under development) should improve bioavailability for preventive and therapeutic use.

In summary, the present study presents a novel mechanism of XN-mediated action. By inducing the $O_2^{-\cdot}$ of mitochondrial origin, followed by disruption of mitochondrial integrity and induction of apoptosis, XN may represent a new member of mitocans. The current findings and future studies will reveal if prooxidant effects are relevant in rodent models of carcinogenesis and will open interesting perspectives in the research on therapeutic strategies by using dietary polyphenols such as Xanthohumol. FJ

Support by the Deutsches Krebsforschungszentrum (DKFZ) Light Microscopy Facility (Heidelberg, Germany) is gratefully acknowledged. The authors thank Dr. Matthew Whiteman for critical reviewing of the manuscript and valuable suggestions.

REFERENCES

1. Kamata, H., and Hirata, H. (1999) Redox regulation of cellular signalling. *Cell. Signal.* **11,** 1–14
2. Fruehauf, J. P., and Meyskens, F. L., Jr. (2007) Reactive oxygen species: a breath of life or death? *Clin. Cancer Res.* **13,** 789–794
3. Boveris, A., and Chance, B. (1973) The mitochondrial generation of hydrogen peroxide. General properties and effect of hyperbaric oxygen. *Biochem. J.* **134,** 707–716
4. Boveris, A., and Cadenas, E. (1975) Mitochondrial production of superoxide anions and its relationship to the antimycin insensitive respiration. *FEBS Lett.* **54,** 311–314
5. Pani, G., Koch, O. R. l., and Galeotti, T. (2009) The p53–p66shc-manganese superoxide dismutase (MnSOD) network: A mitochondrial intrigue to generate reactive oxygen species. *Int. J. Biochem. Cell Biol.* **41,** 1002–1005
6. Orrenius, S., Gogvadze, V., and Zhivotovsky, B. (2007) Mitochondrial oxidative stress: implications for cell death. *Annu. Rev. Pharmacol. Toxicol.* **47,** 143–183
7. Lau, A. T., Wang, Y., and Chiu, J. F. (2008) Reactive oxygen species: current knowledge and applications in cancer research and therapeutic. *J. Cell. Biochem.* **104,** 657–667
8. Klaunig, J. E., and Kamendulis, L. M. (2004) The role of oxidative stress in carcinogenesis. *Annu. Rev. Pharmacol. Toxicol.* **44,** 239–267
9. Droge, W. (2002) Free radicals in the physiological control of cell function. *Physiol. Rev.* **82,** 47–95
10. Green, D. R., and Reed, J. C. (1998) Mitochondria and apoptosis. *Science* **281,** 1309–1312
11. Desagher, S., and Martinou, J. C. (2000) Mitochondria as the central control point of apoptosis. *Trends Cell. Biol.* **10,** 369–377
12. Simon, H. U., Haj-Yehia, A., and Levi-Schaffer, F. (2000) Role of reactive oxygen species (ROS) in apoptosis induction. *Apoptosis* **5,** 415–418
13. Yuen, B., Furrer, L., and Ballmer, P. E. (2005) [Antioxidant vitamin supplementation in the prevention of cardiovascular disease]. *Ther. Umsch.* **62,** 615–618
14. Ladas, E. J., Jacobson, J. S., Kennedy, D. D., Teel, K., Fleischauer, A., and Kelly, K. M. (2004) Antioxidants and cancer therapy: a systematic review. *J. Clin. Oncol.* **22,** 517–528
15. Trachootham, D., Alexandre, J., and Huang, P. (2009) Targeting cancer cells by ROS-mediated mechanisms: a radical therapeutic approach? *Nat. Rev. Drug Discov.* **8,** 579–591
16. Khan, N., Afaq, F., and Mukhtar, H. (2008) Cancer chemoprevention through dietary antioxidants: progress and promise. *Antioxid. Redox Signal.* **10,** 475–510
17. Lee, K. W., and Lee, H. J. (2006) The roles of polyphenols in cancer chemoprevention. *Biofactors* **26,** 105–121
18. Antosiewicz, J., Ziolkowski, W., Kar, S., Powolny, A. A., and Singh, S. V. (2008) Role of reactive oxygen intermediates in cellular responses to dietary cancer chemopreventive agents. *Planta Med.* **74,** 1570–1579
19. Gerhauser, C., Alt, A., Heiss, E., Gamal-Eldeen, A., Klimo, K., Knauft, J., Neumann, I., Scherf, H. R., Frank, N., Bartsch, H., and Becker, H. (2002) Cancer chemopreventive activity of xanthohumol, a natural product derived from hop. *Mol. Cancer Ther.* **1,** 959–969
20. Gerhauser, C. (2005) Beer constituents as potential cancer chemopreventive agents. *Eur. J. Cancer* **41,** 1941–1954
21. Strathmann, J., Klimo, K., Steinle, R., Hussong, R., Frank, N., and Gerhauser, C. (2009) Xanthohumol from hops prevents hormone-dependent tumorigenesis in vitro and in vivo. *Acta Hort.* **848,** 179–190
22. Pan, L., Becker, H., and Gerhauser, C. (2005) Xanthohumol induces apoptosis in cultured 40-16 human colon cancer cells by activation of the death receptor- and mitochondrial pathway. *Mol. Nutr. Food Res.* **49,** 837–843
23. Yang, J. Y., la-Fera, M. A., Rayalam, S., and Baile, C. A. (2007) Effect of xanthohumol and isoxanthohumol on 3T3-L1 cell apoptosis and adipogenesis. *Apoptosis* **12,** 1953–1963
24. Monteghirfo, S., Tosetti, F., Ambrosini, C., Stigliani, S., Pozzi, S., Frassoni, F., Fassina, G., Soverini, S., Albini, A., and Ferrari, N. (2008) Antileukemia effects of xanthohumol in Bcr/Abl-transformed cells involve nuclear factor-kappaB and p53 modulation. *Mol. Cancer Ther.* **7,** 2692–2702
25. Lust, S., Vanhoecke, B., Van Gele, M., Boelens, J., Van Melckebeke, H., Kaileh, M., Vanden Berghe, W., Haegeman, G., Philippe, J., Bracke, M., and Offner, F. (2009) Xanthohumol activates the proapoptotic arm of the unfolded protein response in chronic lymphocytic leukemia. *Anticancer Res.* **29,** 3797–3805
26. Ralph, S. J., and Neuzil, J. (2009) Mitochondria as targets for cancer therapy. *Mol. Nutr. Food Res.* **53,** 9–28
27. Hayward, S. W., Dahiya, R., Cunha, G. R., Bartek, J., Deshpande, N., and Narayan, P. (1995) Establishment and characterization of an immortalized but non-transformed human prostate epithelial cell line: BPH-1. *In Vitro Cell. Dev. Biol. Anim.* **31,** 14–24
28. Dussmann, H., Kogel, D., Rehm, M., and Prehn, J. H. (2003) Mitochondrial membrane permeabilization and superoxide production during apoptosis. A single-cell analysis. *J. Biol. Chem.* **278,** 12645–12649
29. Frezza, C., Cipolat, S., and Scorrano, L. (2007) Organelle isolation: functional mitochondria from mouse liver, muscle and cultured fibroblasts. *Nat. Protoc.* **2,** 287–295
30. Pappa, G., Bartsch, H., Gerhauser, C. (2007) Biphasic modulation of cell proliferation by sulforaphane at physiologically relevant exposure times in a human colon cancer cell line. *Mol. Nutr. Food Res.* **51,** 977–984
31. King, M. P., and Attardi, G. (1996) Isolation of human cell lines lacking mitochondrial DNA. *Methods Enzymol.* **264,** 304–313
32. Kaminski, M., Kiessling, M., Suss, D., Krammer, P. H., and Gulow, K. (2007) Novel role for mitochondria: protein kinase Ctheta-dependent oxidative signaling organelles in activation-induced T-cell death. *Mol. Cell. Biol.* **27,** 3625–3639

33. Kolker, S., Schwab, M., Horster, F., Sauer, S., Hinz, A., Wolf, N. I., Mayatepek, E., Hoffmann, G. F., Smeitink, J. A., and Okun, J. G. (2003) Methylmalonic acid, a biochemical hallmark of methylmalonic acidurias but no inhibitor of mitochondrial respiratory chain. *J. Biol. Chem.* **278,** 47388–47393
34. Sauer, S. W., Okun, J. G., Hoffmann, G. F., Koelker, S., and Morath, M. A. (2008) Impact of short- and medium-chain organic acids, acylcarnitines, and acyl-CoAs on mitochondrial energy metabolism. *Biochim. Biophys. Acta* **1777,** 1276–1282
35. Pappa, G., Lichtenberg, M., Iori, R., Barillari, J., Bartsch, H., and Gerhauser, C. (2006) Comparison of growth inhibition profiles and mechanisms of apoptosis induction in human colon cancer cell lines by isothiocyanates and indoles from Brassicaceae. *Mutat. Res.* **599,** 76–87
36. Skehan, P., Storeng, R., Scudiero, D., Monks, A., McMahon, J., Vistica, D., Warren, J. T., Bokesch, H., Kenney, S., and Boyd, M. R. (1990) New colorimetric cytotoxicity assay for anticancer-drug screening. *J. Natl. Cancer Inst.* **82,** 1107–1112
37. Pappa, G., Strathmann, J., Lowinger, M., Bartsch, H., and Gerhauser, C. (2007) Quantitative combination effects between sulforaphane and 3,3′-diindolylmethane on proliferation of human colon cancer cells in vitro. *Carcinogenesis* **28,** 1471–1477
38. Halliwell, B., and Whiteman, M. (2004) Measuring reactive species and oxidative damage in vivo and in cell culture: how should you do it and what do the results mean? *Br. J. Pharmacol.* **142,** 231–255
39. Zhao, H., Joseph, J., Fales, H. M., Sokoloski, E. A., Levine, R. L., Vasquez-Vivar, J., and Kalyanaraman, B. (2005) Detection and characterization of the product of hydroethidine and intracellular superoxide by HPLC and limitations of fluorescence. *Proc. Natl. Acad. Sci. U. S. A.* **102,** 5727–5732
40. Bellion, P., Olk, M., Will, F., Dietrich, H., Baum, M., Eisenbrand, G., and Janzowski, C. (2009) Formation of hydrogen peroxide in cell culture media by apple polyphenols and its effect on antioxidant biomarkers in the colon cell line HT-29. *Mol. Nutr. Food Res.* **53,** 1226–1236
41. Franco, R., and Cidlowski, J. A. (2009) Apoptosis and glutathione: beyond an antioxidant. *Cell Death Differ.* **16,** 1303–1314
42. Galati, G., Sabzevari, O., Wilson, J. X., and O'Brien, P. J. (2002) Prooxidant activity and cellular effects of the phenoxyl radicals of dietary flavonoids and other polyphenolics. *Toxicology* **177,** 91–104
43. Rehm, M., Dussmann, H., and Prehn, J. H. (2003) Real-time single cell analysis of Smac/DIABLO release during apoptosis. *J. Cell Biol.* **162,** 1031–1043
44. Knudson, C. M., and Brown, N. M. (2008) Mitochondria potential, bax "activation," and programmed cell death. *Methods Mol. Biol.* **414,** 95–108
45. Cai, J., and Jones, D. P. (1998) Superoxide in apoptosis. Mitochondrial generation triggered by cytochrome c loss. *J. Biol. Chem.* **273,** 11401–11404
46. Storz, P. (2006) Reactive oxygen species-mediated mitochondria-to-nucleus signaling: a key to aging and radical-caused diseases. *Sci. STKE* 2006, re3
47. Perez, C. A., Wei, Y., and Guo, M. (2009) Iron-binding and anti-Fenton properties of baicalein and baicalin. *J. Inorg. Biochem.* **103,** 326–332
48. Guo, M., Perez, C., Wei, Y., Rapoza, E., Su, G., Bou-Abdallah, F., and Chasteen, N. D. (2007) Iron-binding properties of plant phenolics and cranberry's bio-effects. *Dalton Trans.* 4951–4961
49. Pang, Y., Nikolic, D., Zhu, D., Chadwick, L. R., Pauli, G. F., Farnsworth, N. R., and van Breemen, R. B. (2007) Binding of the hop (*Humulus lupulus* L.) chalcone xanthohumol to cytosolic proteins in Caco-2 intestinal epithelial cells. *Mol. Nutr. Food Res.* **51,** 872–879
50. Harikumar, K. B., Kunnumakkara, A. B., Ahn, K. S., Anand, P., Krishnan, S., Guha, S., and Aggarwal, B. B. (2009) Modification of the cysteine residues in IkappaBalpha kinase and NF-kappaB (p65) by xanthohumol leads to suppression of NF-kappaB-regulated gene products and potentiation of apoptosis in leukemia cells. *Blood* **113,** 2003–2013
51. Garrido, C., Galluzzi, L., Brunet, M., Puig, P. E., Didelot, C., and Kroemer, G. (2006) Mechanisms of cytochrome c release from mitochondria. *Cell Death Differ.* **13,** 1423–1433
52. Lim, H. W., Lim, H. Y., and Wong, K. P. (2009) Uncoupling of oxidative phosphorylation by curcumin: Implication of its cellular mechanism of action. *Biochem. Biophys. Res. Commun.* **389,** 187–192
53. Ligeret, H., Barthelemy, S., Zini, R., Tillement, J. P., Labidalle, S., and Morin, D. (2004) Effects of curcumin and curcumin derivatives on mitochondrial permeability transition pore. *Free Radic. Biol. Med.* **36,** 919–929
54. Terada, H. (1990) Uncouplers of oxidative phosphorylation. *Environ. Health Perspect.* **87,** 213–218
55. Kowaltowski, A. J., Castilho, R. F., and Vercesi, A. E. (2001) Mitochondrial permeability transition and oxidative stress. *FEBS Lett.* **495,** 12–15
56. Edinger, A. L. and, Thompson, C. B. (2004) Death by design: apoptosis, necrosis and autophagy. *Curr. Opin. Cell. Biol.* **16,** 663–669
57. Maiuri, M. C., Zalckvar, E., Kimchi, A., and Kroemer, G. (2007) Self-eating and self-killing: crosstalk between autophagy and apoptosis. *Nat. Rev. Mol. Cell. Biol.* **8,** 741–752
58. Gozuacik, D., and Kimchi, A. (2004) Autophagy as a cell death and tumor suppressor mechanism. *Oncogene* **23,** 2891–2906
59. Chen, Y., McMillan-Ward, E., Kong, J., Israels, S. J., and Gibson, S. B. (2007) Mitochondrial electron-transport-chain inhibitors of complexes I and II induce autophagic cell death mediated by reactive oxygen species. *J. Cell Sci.* **120,** 4155–4166
60. Chen, Y., Azad, M. B., and Gibson, S. B. (2009) Superoxide is the major reactive oxygen species regulating autophagy. *Cell Death Differ.* **16,** 1040–1052
61. Pervaiz, S., and Clement, M. V. (2002) A permissive apoptotic environment: function of a decrease in intracellular superoxide anion and cytosolic acidification. *Biochem. Biophys. Res. Commun.* **290,** 1145–1150
62. Blair, I. A. (2006) Endogenous glutathione adducts. *Curr. Drug Metab.* **7,** 853–872
63. Valko, M., Morris, H., and Cronin, M. T. (2005) Metals, toxicity and oxidative stress. *Curr. Med. Chem.* **12,** 1161–1208
64. Benhar, M., Engelberg, D., and Levitzki, A. (2002) ROS, stress-activated kinases and stress signaling in cancer. *EMBO Rep.* **3,** 420–425
65. Reddy, V. P., Zhu, X., Perry, G., and Smith, M. A. (2009) Oxidative stress in diabetes and Alzheimer's disease. *J. Alzheimers Dis.* **16,** 763–774
66. Neuzil, J., Wang, X. F., Dong, L. F., Low, P., and Ralph, S. J. (2006) Molecular mechanism of "mitocan"-induced apoptosis in cancer cells epitomizes the multiple roles of reactive oxygen species and Bcl-2 family proteins. *FEBS Lett.* **580,** 5125–5129
67. Schumacker, P. T. (2006) Reactive oxygen species in cancer cells: live by the sword, die by the sword. *Cancer Cell* **10,** 175–176
68. Trachootham, D., Zhou, Y., Zhang, H., Demizu, Y., Chen, Z., Pelicano, H., Chiao, P. J., Achanta, G., Arlinghaus, R. B., Liu, J., and Huang, P. (2006) Selective killing of oncogenically transformed cells through a ROS-mediated mechanism by beta-phenylethyl isothiocyanate. *Cancer Cell* **10,** 241–252
69. Hussong, R., Frank, N., Knauft, J., Ittrich, C., Owen, R., Becker, H., and Gerhauser, C. (2005) A safety study of oral xanthohumol administration and its influence on fertility in Sprague Dawley rats. *Mol. Nutr. Food Res.* **49,** 861–867

Received for publication January 25, 2010.
Accepted for publication February 25, 2010.

XANTHOHUMOL-INDUCED TRANSIENT SUPEROXIDE ANION RADICAL FORMATION TRIGGERS CANCER CELLS INTO APOPTOSIS VIA A MITOCHONDRIA-MEDIATED MECHANISM

Julia Strathmann[1], Karin Klimo[1], Sven W. Sauer[2], Jürgen G. Okun[2], Jochen H.M. Prehn[3], Clarissa Gerhäuser[1]

Supplementary Material

SUPPLEMENTARY MATERIALS AND METHODS

Determination of 'generalized oxidative stress'. Cells were seeded in 96-well plates and grown overnight. After removal of cell culture media, cells were once washed with PBS, and 190µl of 25µM 2',7'-dichlorodihydrofluorescein diacetate (H_2DCF-DA) dissolved in PBS were added to each well. Immediately before starting the measurement, 10µl of XN or solvent control (10% DMSO, 0.5% final concentration) were added, and the time-dependent increase in fluorescence (Ex/Em: 480/520 nm) was measured using a CytoFluor series 4000 multi well plate reader (PerSeptive Biosystems, Freiburg, Germany) for 20 min at 37°C.

XN phenoxylradical formation. Oxygen consumption as an indication of XN phenoxylradical formation in the presence of GSH, H_2O_2, and 0.1U of HRP was monitored using a Clark-type oxygen electrode as published previously (1).

Isolation of mouse liver mitochondria and determination of mitochondrial respiration. Mitochondria were isolated from livers of male FVB/N mice, 4-6 months of age, which were starved over night, essentially as described earlier (Frezza et al., 2007). Respiration was measured by monitoring oxygen consumption using a Clark-type oxygen electrode according to Frezza et al. (2). To test inhibition of mitochondrial respiration, XN or Antimycin A at a concentration of 100 µM (with a final DMSO concentration of less than 0.03%) was added, and respiration was recorded for another minute.

Iron-binding capacity of XN. Titration of Xanthohumol binding to Fe^{2+}, Fe^{3+} and haemin in 20mM potassium phosphate buffer, pH 7.2, was carried out as published elsewhere (3).

Thiol determination in isolated mitochondria. Reducced thiol content was measured according to (4), using 5,5'-dithiobis(nitrobenzoic acid) (Ellman's reagent). Values were normalized to a GSH standard curve ranging from 0 to 500µM.

Supplementary Figure S1:

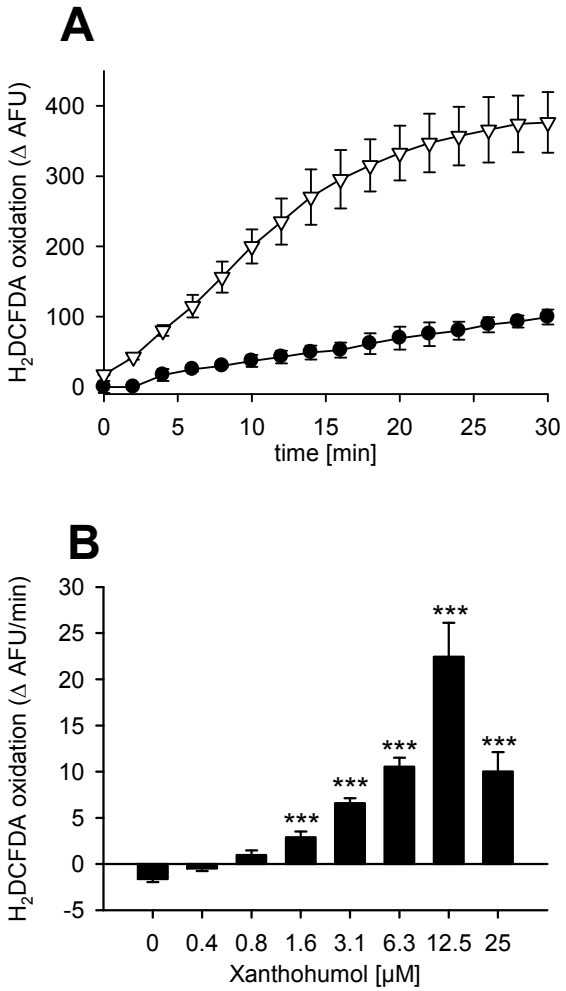

Suppl. Figure S1: XN transiently induces 'generalized oxidative stress' in a time- and dose-dependent manner. (A): Time-dependent increase in H_2DCF-DA oxidation in BPH-1 cells, indicative of generalized oxidative stress after treatment with XN at a concentration of 12.5 µM. Control (●), XN (▽). (B): Dose-dependent increase in H_2DCF-DA oxidation after 10min of treatment with XN. Data are expressed as a fold increase in AFU in relation to the solvent control. Mean ± SD (standard deviation), n=3. *** $p < 0.001$, determined by univariant analysis of variance (ANOVA).

Supplementary Figure S2:

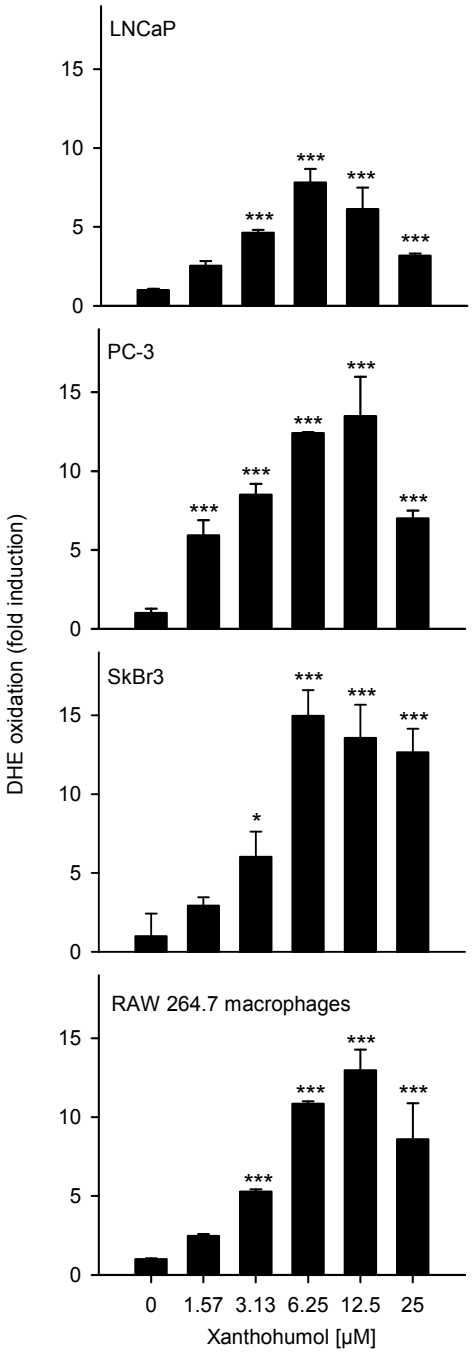

Suppl. Figure S2: Dose-dependent induction of $O_2^{-\bullet}$ in LNCaP and PC-3 human prostate cancer cell lines, SkBr3 human breast cancer cells, and RAW 264.7 murine macrophages, measured by DHE oxidation after 10 min of XN-treatment. Data are expressed as a fold increase in AFU in relation to the solvent control. Mean ± SD, n=3. * $p < 0.05$, *** $p < 0.001$, determined by univariant analysis of variance (ANOVA).

Supplementary Figure S3:

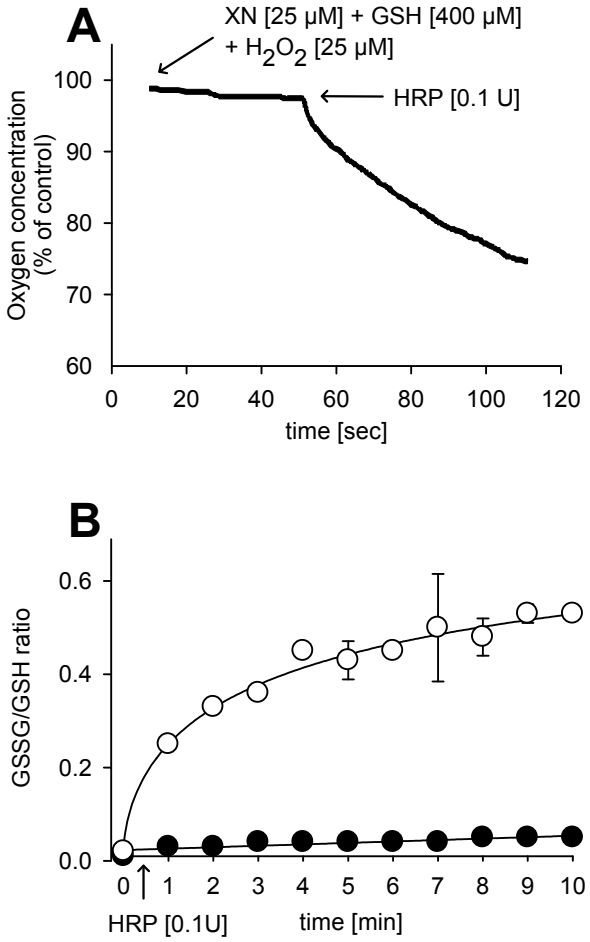

Suppl. Figure S3: XN oxidation to a phenoxyl radical and GSH co-oxidation. (A): Time-dependent oxygen consumption measured using a Clark-Type Oxygen Electrode during oxidation of XN by horse radish peroxidase (HRP) in the presence of GSH and catalytic amounts of H_2O_2. (B): Co-oxidation of GSH during oxidation of XN by HRP, in the presence of 25µM H_2O_2 and 400µM GSH (● control, ○ XN). Mean ± SD, n=3.

Supplementary Figure S4:

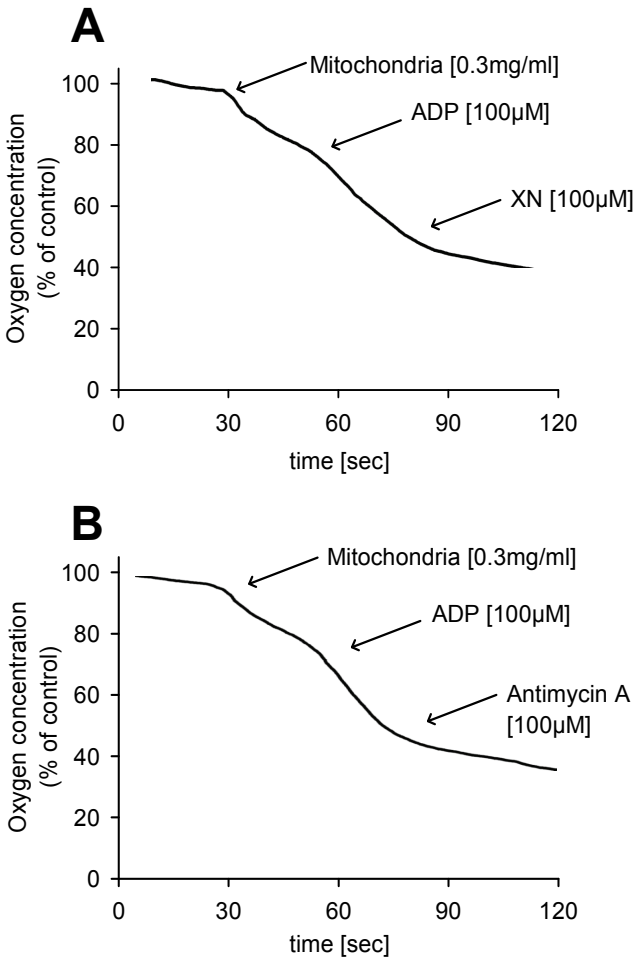

Suppl. Figure S4: Representative images of inhibition of mitochondrial respiration by XN (A) and Antimycin A (B), measured by oxygen consumption with a Clark-type oxygen electrode.

Supplementary Figure S5:

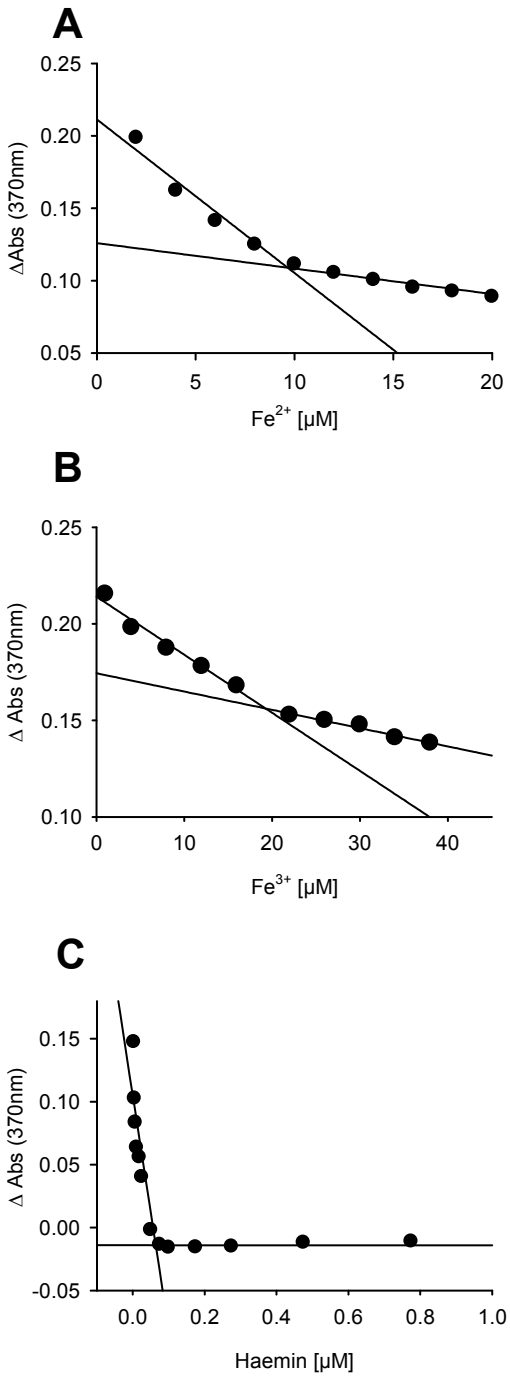

Suppl. Figure S5: Titration of XN at a concentration of 10μM in the presence of (A) Fe^{2+}, (B) Fe^{3+} and (C) haemin. (A): Absorbance of XN-Fe^{2+} complex at 370 nm *versus* Fe^{2+} concentrations, (B): XN-Fe^{3+} complex at 370 nm *versus* Fe^{3+} concentrations and (C): XN-haemin complex at 370 nm *versus* haemin.

These titrations indicate that XN most likely forms complexes with Fe^{2+} and Fe^{3+} in a ratio of 1:1 and 1:2, respectively. Titration of XN with haemin suggests a shift in π-electrons of XN, resulting in an immediate loss of absorption of XN.

Supplementary Figure S6:

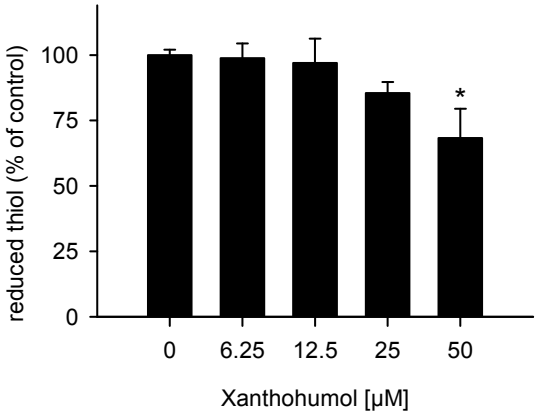

Suppl. Figure S6: Thiol group oxidation in isolated mitochondria after 15 min of XN-treatment. Thiol values were ranging from 255.2 – 344.2 nmol/mg protein. Mean ± SD, n=3, * $p < 0.05$, ANOVA.

SUPPLEMENTARY REFERENCE LIST

1. Galati, G., Sabzevari, O., Wilson, J. X., O'Brien, P. J. (2002) Prooxidant activity and cellular effects of the phenoxyl radicals of dietary flavonoids and other polyphenolics. *Toxicology* 177, 91-104

2. Frezza, C., Cipolat, S., Scorrano, L. (2007) Organelle isolation: functional mitochondria from mouse liver, muscle and cultured fibroblasts. *Nat.Protoc.* 2, 287-295

3. Guo, M., Perez, C., Wei, Y., Rapoza, E., Su, G., Bou-Abdallah, F., Chasteen, N. D. (2007) Iron-binding properties of plant phenolics and cranberry's bio-effects. *Dalton Trans.* 4951-4961

4. Ligeret, H., Barthelemy, S., Zini, R., Tillement, J. P., Labidalle, S., Morin, D. (2004) Effects of curcumin and curcumin derivatives on mitochondrial permeability transition pore. *Free Radic.Biol.Med.* 36, 919-929